# Characterisation of porosity and sensor response times of sol-gel-derived thin films for oxygen sensor applications

by
Philip Bowe B.Sc. (HONS.)

Submitted for the Degree of
**Master of Science**

Presented to
**Dublin City University**

Research Supervisor
**Prof. Brian D. MacCraith,**
**School of Physical Sciences,**
**Dublin City University.**

**JANUARY 2003**

## Declaration

I hereby certify that this material, which I now submit for assessment on the programme of study leading to the award of Master of Science is entirely my own work and has not been taken from the work of others save and to the extent that such work has been cited and acknowledged within the text of my work.

Signed:.....

ID Number:.....

Date:.....

## Dedication

I would like to dedicate this to my parents, Ned and Marguerite.

## Acknowledgements

I would like to thank all the members of the Optical Sensors Group for making my time here most enjoyable.
I would also like to thank Dr. Colette McDonagh for all her invaluable help throughout my masters.
Finally I would like to thank Prof. Brian MacCraith for giving me this brilliant opportunity.

## Abstract

The ability to determine oxygen concentration is of great importance in many industrial, environmental and medical applications. In recent years, a range of sol-gel-derived optical oxygen sensors, for measuring oxygen in both gas and aqueous phase has been developed, in which the oxygen sensitive dye Ru(II)-tris(4,7 - diphenyl-1,10-phenanthroline) has been entrapped. The porosity of the matrix plays a vital role in determining both the sensitivity and response time of such optical sensors. For gas sensors, the diffusion coefficient for the analyte gas through the matrix increases with film porosity. This in turn increases the sensitivity of the sensor response via the Stern-Volmer coefficient. The response and recovery times are also related to porosity via the diffusion coefficient.

This project focuses on the fabrication of a wide range of sol-gel-derived thin films as well as the development of experimental systems used to calculate the porosity and response times of a wide range of sol-gel-derived thin films. A method to calculate the diffusion coefficient using response and recovery times as well as film thickness is also detailed. Measured response times were correlated with porosity, Stern-Volmer coefficients and diffusion coefficients data. The Stern-Volmer equation was also used to characterise and explain specific film behavior. A fabrication method used to control the refractive index of sol-gel thin films is also detailed and the consequence this has on the film characteristics is investigated.

# Contents

# List of Figures

# List of Tables

# Chapter 1

# Introduction

## 1.1 Introduction

There are many different families of sensors such as mechanical, electrical, thermal and electrochemical, but the sensors of interest in this work are optical chemical sensors with particular emphasis on optical oxygen sensors. This work is based on the investigation of sol-gel materials for use as optical oxygen sensors. The sol-gel glass is doped with a ruthenium dye complex whose fluorescence is quenched in the presence of oxygen. In this chapter, a brief description is given of optical chemical sensors, focussing, in particular, on sol-gel based sensors. The objectives along with the outline of the thesis are also presented.

## 1.2 Optical Chemical sensors

By definition, a sensor is a device that is able to indicate continuously and reversibly the concentration of an analyte or a physical parameter. An optical sensor uses light and changes in light to measure and detect the presence or concentration of an analyte. Depending on the origin of the optical signal, optical chemical sensors are classified as absorption, fluorescence, phosphorescence, Raman or infrared sensors. Fluorescence-based sensing is far superior to absorption-based sensing because of its higher sensitivity, selectivity and compatibility with laser excitation systems. Numerous organic and inorganic analytes have been shown to be fluorescent under irradiation or to be determinable via a fluorogenic reaction. The increasing availability and suitability of LEDs and sensitive photodetectors allow their use in simple,

low-cost and safe instrumentation. Optical sensing can offer some of the following advantages over other sensor types [1, 2]:

1. Ease of fabrication allows the development of very small, light and flexible sensors.

2. Because the primary signal is optical, it is not subject to electrical interference.

3. The use of optical fibres allows the transmission of light over large distances making remote sensing possible.

4. Many sensors are simple in design and can be fabricated from low cost materials. This opens the way for disposable sensors.

5. Optical sensors have been developed which respond to chemical analytes or physical parameters for which electrodes are not available.

However, optical chemical sensors do exhibit the following disadvantages:

1. The reagents used can be prone to photobleaching and leaching leading to instability in output signal.

2. Ambient light can interfere if lock-in detection and suitable filters are not used.

There has been much work done and numerous papers published on optical oxygen sensing. One of the first oxygen sensors was developed by Bergman [3]. His work was based on the quenching by oxygen of fluoranthene that was incorporated in a porous vycor glass. Oxygen quenching of fluorescence of dyes was first reported in the 1930's by Kautsky [4]. In this paper he explained the mechanism of fluorescence quenching by oxygen. The dye complex is excited by light at a certain wavelength. While in this excited state, oxygen molecules collide with it and a charge transfer complex is formed. Energy is transferred to the oxygen and non-radiative decay occurs. No oxygen is consumed during this process and it is fully reversible. The quenching of fluorescence can be correlated with oxygen concentration.

Luminescent transition metal complexes , especially ruthenium poly(pyridyl) compounds, are suitable for oxygen sensing [5], because of their high emissive metal-ligand charge transfer, long fluorescence lifetime, large Stokes shift, high quenching efficiencies and absorption in the blue region of the spectrum. These complexes have been extensively studied [6] and will be discussed in detail in Chapter 3.

Optical chemical sensors usually require immobilisation of the appropriate reagent on an optical fibre or waveguide [7]. Although sol-gel immobilisation is the focus of this work, other sensors have their indicator phase immobilised in a polymer membrane [8]. However it has been found that polymers have a number of disadvantages which affect their suitability as a support matrix [9]. Polymers have a degradation problem when exposed to environments containing organic solvents and temperatures in excess of 60°C. They also have serious deformation problems after swelling.

## 1.3 The sol-gel process and sol-gel sensors

Sol-gel processing involves hydrolysis and condensation of precursors at low temperatures to form porous glass. By the manipulation of the processing parameters the glasses can be fabricated with specific properties [10]. The initial sol containing the precursor is liquid, hence the production of very thin films is possible by a number of different coating techniques, such as dip-coating, spin-coating and aerosol deposition [11, 12, 13, 14].

Sol-gel derived thin films can be used in a wide range of applications, including electrical [15], sensor applications [5, 16, 17, 18, 19, 20, 21], optical gain media and non-linear applications [22, 23, 24].

In the area of optical sensors the primary use of sol-gel materials is as a method of immobilisation of reagents. The analyte-sensitive reagent is entrapped within the sol-gel matrix and smaller analyte molecules may diffuse through the porous matrix and interact with the reagent [17].

The sol-gel technique offers many advantages over other immobilisation techniques for the fabrication of chemically sensitive supports [25].

1. The glasses are chemically inert, photostable and thermally stable, making them highly suitable for applications in harsh environments.

2. The preparation of doped glass is technically simple. The trapping procedure is straightforward, compared to, for example, the covalent binding of a reagent to a solid support.

3. The flexibility of the process enables a range of critical sensor parameters to be optimised. For example, film thickness can be controlled accurately by the

withdrawal speed of the substrate from the sol-gel solution.

4. The technique is particularly suited to gas sensing because the high specific area (e.g., $100m^2/g$) of the microporous structure enhances the sensitivity.

The Optical Sensors Laboratory at Dublin City University has a long history in the production of optical sol-gel based sensors. These sensors were employed in the detection of a range of gases including, ammonia, oxygen and carbon dioxide [5, 7, 16, 17, 18, 19, 20].

## 1.4 Objectives

This work deals with the optimisation of optical oxygen sensors employing doped sol-gel films. Response time, porosity and diffusion coefficient are three very important characteristics of thin film oxygen sensors, and affect greatly the sensor performance. The sol-gel thin films used in this work are in the order of 400nm in thickness with submicron pore sizes. The principal objectives of this work were:

1. To develop and perfect an experimental system for measuring the porosity of sol-gel films.

2. To develop an experimental system for measuring the subsecond response times of sol-gel oxygen sensitive films.

3. To develop a computer model capable of calculating the diffusion coefficient of a sol-gel thin film using the response and recovery times, as well as the thickness of the film.

4. To fabricate and characterise a wide range of sol-gel films, using different fabrication parameters.

5. To investigate the relationship between response time, porosity and diffusion coefficient and attempt to explain how sensor behavior depends on these important characteristics.

## 1.5 Outline of the thesis

The background of optical chemical sensors and the use of a sol-gel material as a support matrix is explained in this chapter. In Chapter 2 the sol-gel process is explained, detailing the fundamental parameters affecting the final structural properties of the sol-gel film.

In Chapter 3 the principles of fluorescence are explained as well as the use of fluorescence quenching for the detection of oxygen. The Stern-Volmer equation is introduced in order to characterise in detail the behavior of oxygen sensitive films. The development of a numerical model to calculate the diffusion coefficient of a sol-gel film is also detailed.

Chapter 4 describes the development of the experimental techniques used throughout this work. The fabrication of a wide range of films used throughout this work is also detailed.

Chapter 5 deals with porosity results obtained from a range sol-gel films fabricated using different tailoring techniques known to control the final porosity of the sol-gel-derived film.

In Chapters 6 and 7, the porosity results, response times and other data such as the Stern-Volmer equation are combined to explain the behavior of sol-gel oxygen sensitive thin films.

In the final chapter the objectives are revisited and conclusions drawn.

# Bibliography


[1] S.G. Schulman. *Molecular Luminescence Spectroscopy: Methods and Applications: Part 2.* John Wiley and Sons, New York, 1988.

[2] S.B. Bambot, R. Holavanahali, J.R. Lakowicz, G.M. Carter, and G.Rao. Phase fluorometric sterilizable optical oxygen sesnor. *Biotechnology and Bioengineering*, 43:1139–1145, 1994.

[3] I. Bergman. Rapid-response atmospheric oxygen monitor based on fluorescence quenching. *Nature*, 218:396, 1968.

[4] H. Kautsky. Quenching of luminescence by oxygen. *Transactions of the Faraday Society*, 35:216–219, 1939.

[5] B.D. MacCraith, C.M. McDonagh, G. O'Keefe, A.K. McEvoy, T. Butler, and F.R. Sheridan. Sol-gel coatings for optical chemical sensors and biosensors. *Sensors and Actuators B*, 29:51–57, 1995.

[6] E.R. Carraway, J.N. Demas, B.A. DeGraff, and J.R. Bacon. Photophysics and photochemistry of oxygen sensors based on luminescent transition-metal complexes. *Analytical Chemistry*, 63:337–342, 1991.

[7] Thomas M. Butler. *Development of Evanescent Wave pH Sensors Based on Coated Optical Fibres.* PhD thesis, Dublin City University, 1996.

[8] T. Furuto, S.K. Lee, Y. Amao, K. Asai, and I. Okura. Oxygen sensing system using triplet reflectance of zinc porphyrin immobilised in polymer membrane studies by laser flash photolysis. *Journal of Photochemistry and Photobiology*, 132:81–86, 2000.

[9] M.R. Shahriari and G.H. Siegal J.Y. Ding, J. Tong. Sol-gel coating based fibre optic oxygen/dissolved oxygen sensors. *Proc SPIE*, 2068:224, 1994.

[10] C.J. Brinker and G.W. Scherer. *Sol-Gel Science: The Physics and Chemistry of Sol-Gel Processing.* Academic Press Inc., San Diego, 1990.

[11] C.J. Brinker, A.J. Hurd, P.R. Schunk, G.C. Frye, and C.S. Ashley. Sol-gel dip coating. *Journal of Non-Crystalline Solids*, 147-148:424–436, 1992.

[12] L.E. Scriven. Physics and applications of dip and spin coating. *Mat. Res. Soc. Symp. Proc.*, 121:717–729, 1988.

[13] K. Vorotilov, V. Petrovsky, and V. Vasiljev. Spin coating process of sol-gel silicate tilms deposition: Effect of spin speed and processing temperture. *Journal of Sol-Gel Science and Technology*, 5:173 183, 1995.

[14] M. Langlet, C. Vautey, and N. Mazeas. Some aspects of the aerosol-gel process. *Thin Solid Films*, 299:25–32, 1997.

[15] K.A. Vorotilov, V.I. Petrovsky, V.A. Vasiljev, and M.V. Sobolevsky. Ormosil films: Properties and microelectric applications. *Journal of Sol-Gel Science and Technology*, 8:581–584, 1997.

[16] A.K. McEvoy, C. McDonagh, and B.D. MacCraith. Optimisation of sol-gel derived silica films for optical oxygen sensing. *Journal of Sol-Gel Science and Technology*, 8:1121–1125, 1997.

[17] G. O'Keeffe, B.D. MacCraith, A.K. McEvoy, C.M. McDonagh, and J.F. McGlip. Development of a led-based phase fluorimetric oxygen sensor using evanescent wave excitation of a sol-gel immobilized dye. *Sensors and Actuators B.*, 29:226–230, 1995.

[18] J.F. Gouin, A. Doyle, and B.D. MacCraith. Fluorescence capture by planar waveguides as platform for optical sensors. *Electronic Letters*, 34:1685–1687, 1998.

[19] P. Lavin, C.M. McDonagh, and B.D. MacCraith. Optimization of ormosil for optical sensor applications. *Journal of Sol-Gel Science and Technology*, 13:641–645, 1998.

[20] O. Worsfold, , C. Malins, M.G. Forkan, I.R. Peterson, B.D. MacCraith, and D.J. Walton. Optical NO2 sensing based on sol-gel entrapped azobenzene dyes. *Sensors and Actuators B-Chemical*, 56(1-2):15–21, 1999.

[21] M.F. Choi and D. Xiao. Single standard calibration for an optical oxygen sensor based on luminescence quenching of a ruthenium complex. *Analytica Chimica Acta*, 403:57–65, 2000.

[22] J. Butty, N. Peyghambarian, Y.H. Kao, and J.D. Mackenzie. Room temperature optical gain in sol-gel derived CdS quantum dots. *Applied Physics Letters*, 69:3224–3226, 1996.

[23] E.M. Yeatman, M.M. Ahmad, O. McCarthy, A. Vannucci, P. Gastaldo, D. Barbier, D. Mongardien, and C. Moronvalle. Optical gain in Er-doped SiO-TiO waveguides fabricated by the sol-gel technique. *Optics Communications*, 164:19–25, 1999.

[24] N. De la Rosa, M. Pinero, R. Litran R, and Y.L. Esquivias. Non-linear optical behaviour of CdS semiconductor nanocrystals inside a silica gel matrix. *Boultein De La Sociedad Espaola De Cermica Y Vidrio*, 39:255–258, 2000.

[25] B.D. MacCraith. Enhanced evanescent wave sensors based on sol-gel derived porous glass coatings. *Sensors and Actuators B*, 11:29–34, 1993.

# Chapter 2

# The Sol-Gel Process

## 2.1 Introduction

The sol-gel process is a method of producing homogeneous glasses and ceramics [1]. The preparation of such materials involves the hydrolysis and polycondensation of metal alkoxides.

The sol-gel method enables one to prepare glasses at far lower temperatures than is possible by using conventional methods. Compositions which are difficult to achieve by conventional means because of high melting temperatures or crystallisation problems can be produced. In addition, the sol-gel process is a high-purity process which leads to excellent homogeneity.

This chapter deals with the principle of sol-gel processing and also describes the different routes available to tailor the films. By controlling particular process parameters, properties such as thickness and porosity can be easily manipulated.

## 2.2 Sol-Gel processing

### 2.2.1 Outline of the process

The principle behind the sol-gel process for making glasses is one of building up reactive units in solution. These units form chains, rings and networks that are later present in the gel. But what exactly is a sol-gel material? A sol is a colloidal suspension of solid particles in a liquid, and is the first phase in the process. Colloids are solid particles with diameters of 1-100nm. A gel is an interconnected, rigid network with pores of submicrometer dimensions and polymeric chains whose aver-

age length is greater than a micrometer. Silica gels can be fabricated in two ways: method 1 involves network growth from an array of discrete colloidal particles, and method 2 involves the formation of an interconnected 3-D network by the simultaneous hydrolysis and polycondensation of an organometallic precursor. Method 2 is used in this work. A precursor is a starting compound which is composed of a metal or a metalloid element surrounded by various ligands. The most common silicon precursor is tetraethoxysilane (TEOS), a silicon alkoxide, where the silicon atom is the central metal ion which is surrounded by four ethoxy groups. Another type of precursor which will be used in this work is an organoalkoxysilane compound, an example of which is methyltriethoxysilane (MTEOS). As before, this compound consists of a central metal ion which is again surrounded by ligands, but in this case one or more of the ligands is an organic group, hence they have direct metal-carbon bonds and not metal-oxygen-carbon bonds as in metal alkoxides.

A sol-gel material is fabricated from the combination of an inorganic or organic (or both) precursor, a catalyst and a solvent such as ethanol. These compounds are mixed well, whereby hydrolysis and polycondensation of the precursor occurs, resulting in the formation of a low density solid gel. This gel can then be subjected to a temperature programme which controls the densification process. A schematic of the process in shown in Figure 2.1.

The process is very well adapted for film formation as, at the sol-gel stage thin glass films can be formed by dip-coating or spin-coating. These films, when dried at relatively low temperatures, are highly porous and are the basis of the sensors discussed in this work.

In the following sections, details of the process will be outlined, and the effect of varying the process parameters with respect to each other will be explained. Firstly, the basic hydrolysis and condensation processes will be described, and then it will be shown how the kinetics of these reactions are strongly influenced by the parameters, and that changing these will change the structure of the sol-gel end-product.

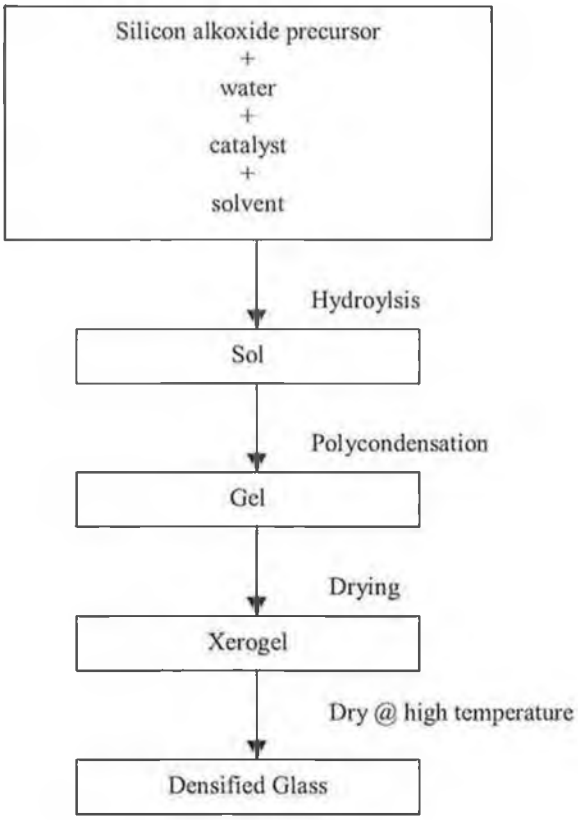


**Figure 2.1:** Outline of sol-gel process for the fabrication of glass

### 2.2.2 Hydrolysis and condensation

A gel is synthesised by hydrolysis and polycondensation of compounds such as alkoxides which are dissolved in alcohol in the presence of water, using a base or acid as a catalyst. Three reactions are generally used to describe the sol-gel process:

$$\text{Hydrolysis: } \equiv \text{Si - OR} + H_2\text{O} \Leftrightarrow \equiv \text{Si - OH} + \text{ROH}$$

$$\text{Alcohol Condensation: } \equiv \text{Si - OR} + \text{HO - Si} \equiv \Leftrightarrow \equiv \text{Si -O - Si} \equiv + \text{ ROH}$$

$$\text{Water Condensation: } \equiv \text{Si - OH} + \text{HO - Si} \equiv \Leftrightarrow \equiv \text{Si - O - Si} \equiv + H_2O$$

where R is an alkyl group $C_xH_{2x+1}$.

The hydrolysis reaction replaces alkoxide groups OR, with the hydroxyl group, OH. This occurs by the nucleophilic attack of oxygen contained in water on the silicon atom [1]. Condensation reactions involving the silanol groups occur via a nucleophilic condensation reaction and produce siloxane bonds, $\equiv Si - O - Si \equiv$, plus the by-products alcohol, ROH and water. Usually condensation starts before hydrolysis is complete. Because water and alkoxysilanes are immiscible, a mutual solvent such as ethanol is used to mix the two together. The ethanol can also take part in the reaction as indicated in the first two reactions. The water and alcohol condensation reactions proceed and build polymeric chains of $\equiv Si - O - Si \equiv$ molecules, which interlink and form networks extending throughout the gel.

### 2.2.3 Aging and drying

Aging is the term given to describe the process after the ingredients have been mixed together to form a sol. Aging usually occurs at elevated temperatures. During the aging period polycondensation and hydrolysis continue. This increases the connectivity of the network. Time, temperature and pH are various parameters that alter the aging process.

Drying is the removal of liquid from the interconnected pore network. The drying process may be divided into three distinct stages [2]. The first stage consists of a decrease in the volume of the gel, which is equal to the volume of the liquid lost by evaporation. The compliant gel network is deformed by the large capillary forces which cause shrinkage of the object. Stage one ends and stage two begins when the "critical point" is reached. The critical point occurs when the strength of the network has increased, due to the greater packing density of the solid phase. This condition creates the highest capillary pressure, and unable to compress the gel any further, the pores begin to empty. Because the rate of evaporation decreases in stage two, classically this is termed "the first falling rate period". The third stage of drying is reached when the pores have substantially emptied. During this period, called the "second falling rate period", there are no further dimensional changes but just a slow progressive loss of weight until equilibrium is reached, determined by the ambient temperature and partial pressure of water.

## 2.3 Factors affecting sol-gel process

### 2.3.1 Influence of water:precursor ratio (R-value)

The R value is the molar ratio of water to silicon alkoxide precursor, [R=($H_2O$) /(precursor)]. It plays a major role in the structural evolution of the sol-gel material. The size of the sol-gel particles and the amount of cross-linking within the sol-gel material is dependent on the R-value [2]. Because water is produced as a by-product of the condensation reaction, an R-value of 2 is theoretically sufficient for complete hydrolysis and condensation to yield anhydrous silica.

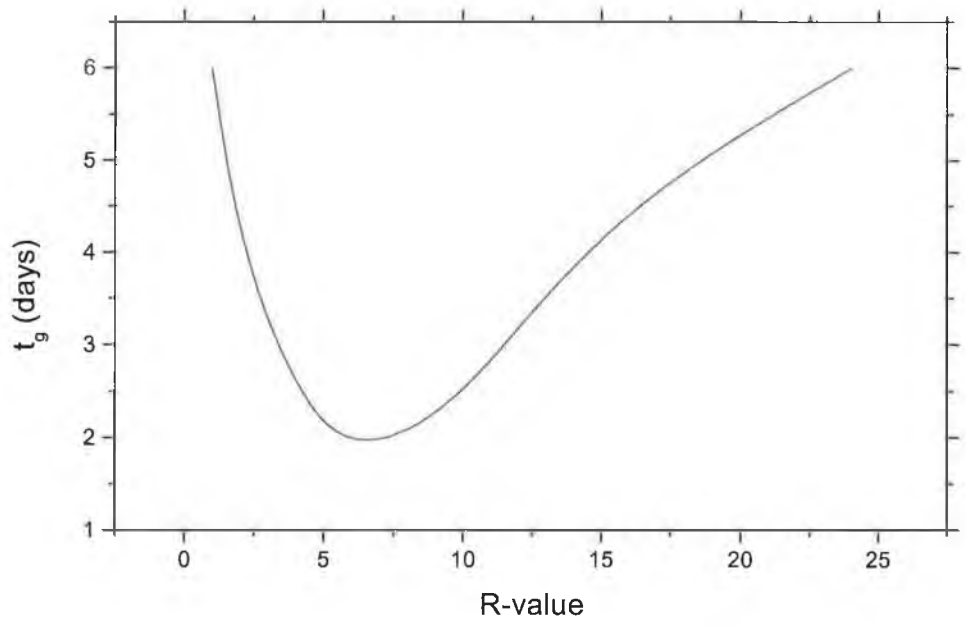


**Figure 2.2:** Variation of the gelation time with R value [1].

However, a value of 2 has been shown to be inadequate for the hydrolysis reaction to proceed to completion [3]. An increased value of R is expected to promote hydrolysis , thus producing a more highly branched polymeric network, but it also slows condensation [4]. Thus an increased value of R will result in a lower sol viscosity, because of both the greater dilution of the sol and the lesser degree of condensation, and therefore a reduced film thickness. It has also been noted that an increase in water content increases the hydrolysis rate for both acid- and base-catalysed sols.

Therefore as R is increased at low pH, more efficient hydrolysis occurs leading to

a decrease in the gel time. The gel time is described as the period of time taken for the liquid sol-gel to form into a solid gel that contains a continuous solid skeleton. As R is increased further there is excess water, the excess water serves to dilute the sol, reducing the relative silica content and giving rise to longer gel times and thinner films with a smaller porosity [4]. Figure 2.2 which shows the dependence of gelation time on R-value, illustrates this point [1].

### 2.3.2 Influence of catalyst type and pH

The pH value of the starting solution is one of the more important parameters in the sol-gel process because it determines whether the process is acid or base catalysed. Acid catalysis is usually associated with fast hydrolysis and relatively long gel times. Acid catalysis produces structures with a fine network structure of linear chains with pore sizes $<$ 2nm. On the otherhand, base catalysis gives slow hydrolysis but the gel times are shorter due to higher condensation rates [1].

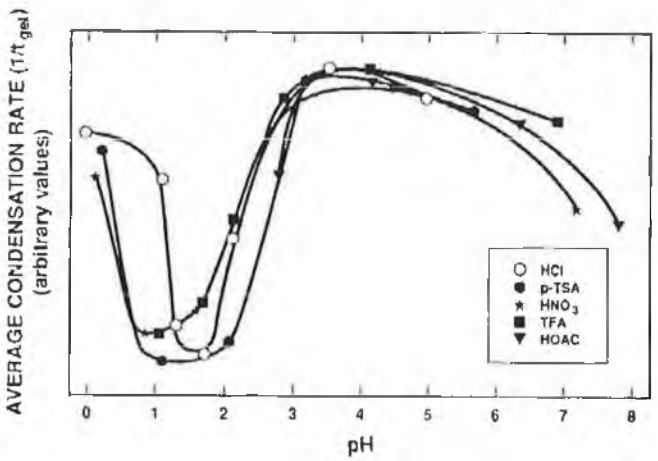


**Figure 2.3:** Average condensation rates (1/gel time) for TEOS hydrolysed with solutions of various acids [1]

Under these conditions more dense colloidal particles are formed with larger pores. For silica, starting solutions of pH $<$ 2 are acid catalysed while solutions of pH $>$ 2 are base catalysed, due to the fact that the isoelectric point of silica (the point at which the electron mobility and surface charge is zero) occurs at approximately pH=2. This pH value defines the boundary between acid and base catalysis in silica

sol-gel processes.

The dependence of the gelation time of sols on the starting solution pH value is clearly illustrated for a range of catalysts in Figure 2.3 [1]. The gel time is equal to 1/(average condensation rate). It can be seen from this plot that the overall condensation rate is minimised between pH values 1.5-2 and maximised approximately at a pH value of 4.

### 2.3.3 Influence of solvent

As already mentioned, because water and alkoxysilanes are immiscible, a mutual solvent such as ethanol is used. Solvents play a role in both hydrolysis and condensation. Solvents may be polar (protic) or non-polar (aprotic). The polarity of the solvent can determine the rate of hydrolysis by increasing or decreasing the catalytic activity.

Ethanol was the polar solvent used in this work. Ethanol has the effect of retarding the gelation process and therefore the gel times increase with ethanol content. This can be seen from Figure 2.4 [1].

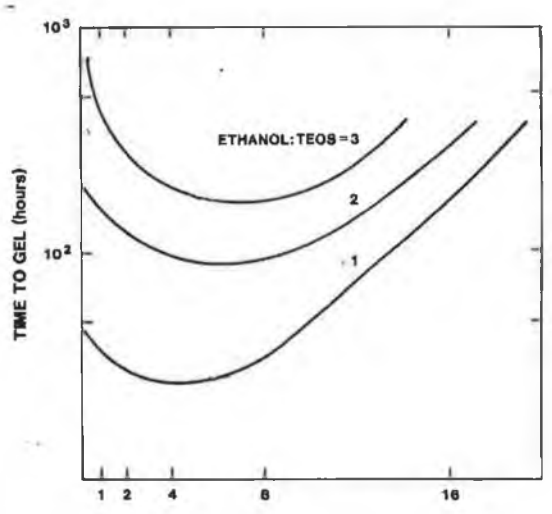


**Figure 2.4:** Effects of TEOS/EtOH ratio on the gelling time for different water concentrations [1]

This retardation in gelation is expected since ethanol is a by-product in both hydrolysis and condensation reactions. Moreover excess alcohol may separate the molecular species formed and hinder cross-linking. Thus with high ethanol content,

the nuclei are kept apart and their growth rate is sluggish. This produces a thin film with tiny pores [5].

## 2.4 Dip-coating process

Dip coating is a simple way of depositing a sol onto a substrate, such as a glass slide. Film thickness is set by the competition of various forces including capillary forces and gravity. Thickness and uniformity can be sensitive to flow conditions in the liquid and the gas overhead. An unusual feature of sol-gel materials is that the faster the substrate is withdrawn the greater the thickness of the film.

The dip coating process can be divided into five stages [6]:immersion, start-up, deposition, drainage and evaporation (see Figure 2.5). The first three are necessarily sequential, the third and fourth, concomitant; the fifth, evaporation of solvent from the liquid, proceeds throughout the process.

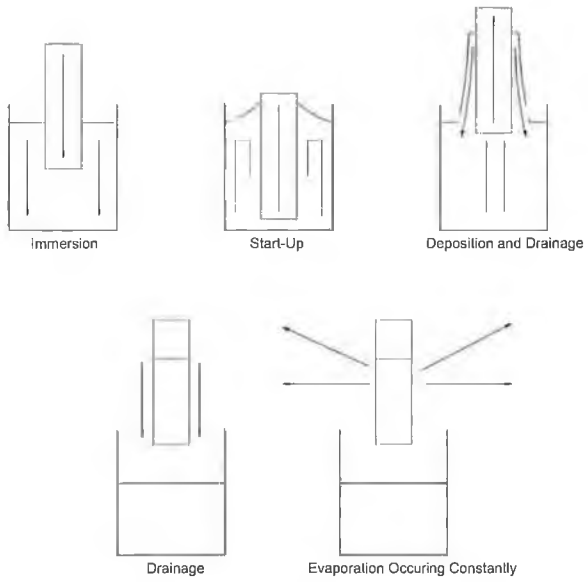


**Figure 2.5:** Stages in the dip coating process.

As the sample is immersed in the liquid and withdrawn, the inner layer of deposited liquid moves in tandem with the substrate while the outer layer returns to the container. The film thickness is related to the position of the dividing border between the upward and the downward moving layers. In the dip coating process there are a number of forces in competition, and these determine the position of the streamline and hence the film thickness. These forces include (1) Viscous drag

upward on the liquid by the moving substrate; (2) force of gravity; (3) resultant force of surface tension in the concavely-shaped meniscus; (4) inertial force of the boundary layer liquid arriving at the deposition region; (5) surface tension gradient; (6) the disjoining or conjoining pressure. The relationship between all these forces is shown below [7]:

$$h = \frac{0.94(\eta U_0)^{\frac{2}{3}}}{\gamma^{\frac{1}{6}}(\rho g)^{\frac{1}{2}}} \tag{2.1}$$

where h is the thickness, $U_0$ is the dip speed, $\eta$ is the liquid viscosity, g is gravity, $\gamma$ is the liquid-vapor surface tension and $\rho$ is the density of the liquid.

## 2.5 Ormosils

Materials formed from tetraethoxysilanes such as TEOS-based sol-gel films, have a hydrophilic surface. The surface has a large coverage of hydroxyl groups, which allow the adsorption of water. However in certain situations this is not the desired effect and a hydrophobic film is required. The use of Ormosils (organically modified silicates) results in the replacement of surface hydroxyls with alkyl groups, which give rise to a hydrophobic surface. A typical example of a modified silicon alkoxide precursor is methyltriethoxysilane (MTEOS, $CH_3(C_2H_5O)_3\mathrm{Si}$), in which a methyl group replaces one of the ethoxy groups. This methyl group is bonded to the silicon atom through a non-hydrolysable covalent bond and has a substantial effect on the surface properties of the film.

Studies of Ormosils have shown that dyes entrapped in organically modified silicate films exhibit less leaching than films prepared from conventual precursors [8]. Furthermore due to enhanced reaction rates, the films are more dense and have smaller average pore sizes [9]. Films of thickness of up to $6\mu m$ are achievable with little or no cracking [10]. Refractive index control is also possible using a combination of organic and inorganic precursors [10].

## 2.6 Encapsulation of molecules within sol-gel matrix

Sol-gel technology enables the production of glasses through chemical reactions at ambient temperatures [11]. As previously explained, sol-gel-derived silica glasses are prepared from the hydrolysis, and condensation polymerisation of a silicon alkoxide solution. The material produced can act as a support matrix for analyte-sensitive dyes which are added to the precursor solution. The dye molecules are trapped in the cage-like structure, but analyte molecules can travel through the interconnected pores, and interact with the analyte-sensitive dye.

This method of doping sol-gel derived glass has been used worldwide to develop sensors to detect a wide range of analytes such as oxygen, carbon dioxide, ammonia and pH [9, 11, 12, 13, 14, 15]

## 2.7 Conclusion

The sol-gel process has been described in detail in this chapter. In particular the chemical processes of hydrolysis and polycondensation, and the variety of fabrication parameters which affect these reactions and determine the final structure of the materials were presented. A description of the chemical modification of these films to remove the surface hydroxyl groups, and render the surface hydrophobic was also described. In conclusion, the sol-gel process is an inexpensive, versatile method to produce sol-gel films having reagents incorporated in them.

[12] A.K. McEvoy, C. McDonagh, and B.D. MacCraith. Optimisation of sol-gel derived silica films for optical oxygen sensing. *Journal of Sol-Gel Science and Technology*, 8:1121–1125, 1997.

[13] B.D. MacCraith, C.M. McDonagh, G. O'Keeffe, A.K. McEvoy, T. Butler, and F.R. Sheridan. Sol-gel coatings for optical chemical sensors and biosensors. *Sensirs and Actuators B*, 29:51–57, 1995.

[14] M.F. Choi and D. Xiao. Single standard calibration for an optical sensor based on luminesence quenching of a ruthenium complex. *Analytica Chimica Acta*, 403:57–65, 2000.

[15] T. Murphy, H. Schmidt, and H-D. Kronfeldt. Use of sol-gel techniques in the development of surface enhanced raman scattering (sers) substrates suitable for in-situ detection of chemicals in sea water. *Applied Physics B*, 69:147–150, 1999.

# Chapter 3

# Principles and characteristics of oxygen sensing

## 3.1 Introduction

Optical oxygen sensors operate on the principle of fluorescence quenching by oxygen. In this chapter the principle of fluorescence quenching is introduced and the mechanism of oxygen detection using a ruthenium complex is outlined.

An important mathematical relationship introduced in this chapter is the Stern-Volmer equation. This equation is explained in detail and its relationship to important characteristics associated with the sensing film is described.

As a consequence of the Stern-Volmer equation, different factors affecting the sensitivity of the oxygen-sensitive films, namely, porosity, permeability, solubility and diffusion coefficient are introduced and explained. In a further investigation of diffusion, a numerical model is developed and used for the calculation of diffusion coefficients.

## 3.2 Introduction to Fluorescence

When a molecule absorbs electromagnetic radiation, the energy is usually lost via collisions in the form of heat. However, with certain molecules, only part of the energy is lost via collisions and the electron drops back to the ground state by emitting a photon of lower energy (longer wavelength) than was absorbed. Figure 3.1 shows a simplified energy level diagram which illustrates the processes of absorption

and emission.

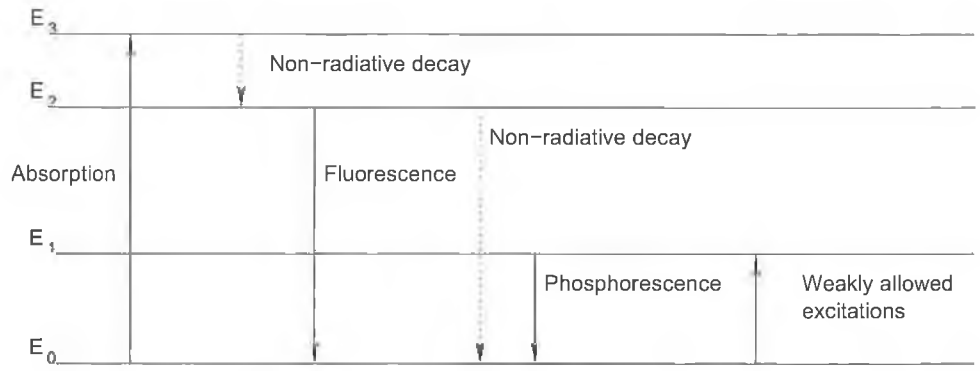


**Figure 3.1:** Generalised energy level diagram illustrating the fundamental excitation and emission processes.

All electrons in a molecule carry a spin angular momentum with a spin quantum number of s=$\frac{1}{2}$. The electron possesses either a spin-up or spin-down property. The total spin angular momentum possessed by a many-electron molecule is the total spin quantum number, S. S is calculated from the vector sum of the individual contributions from each electron [1].

Two electrons each possessing s=$\frac{1}{2}$ may be present with their spins parallel or opposed. If the spins are opposed the total spin quantum number, S, is zero. If the spins are parallel, the total quantum number, S, is $\frac{1}{2} + \frac{1}{2} = 1$. The spin multiplicity gives the number of expected states expected in the presence of an applied magnetic field and is given by 2S+1 [2]. Thus a molecule with all electrons paired according to spin possesses S=0 and a spin multiplicity of 1. Such an electronic state is referred to as a singlet state. The combination of a ground and singlet state is abbreviated by the symbol, $S_0$, this corresponds to $E_0$ in Figure 3.1. If a molecule with a ground state energy level, $E_0$, is excited by an incoming photon, it can be raised to an excited state $E_3$. The absorbed energy can be released either radiatively or non-radiatively. If the gap between $E_3$ and $E_2$ is small, the electron in the excited state tends to decay non-radiatively by phonon emission, releasing energy as heat to the material. Radiative decay occurs either from the singlet, $E_2$, or the triplet state, $E_1$. Fluorescence is the emission resulting from the return of the electron to the ground state, if this transition originates in a singlet state. Such transitions are quantum mechanically allowed, with emission rates as high as $10^8$ per second, and consequently fluorescence lifetimes of approximately 10ns [2]. Emission can also

occur when a triplet state excited electron, $E_1$, returns to a ground state, $E_0$. This is known as phosphorescence. These transitions between states of different multiplicity are quantum mechanically forbidden, but in some molecules are weakly allowed. This happens when the molecule contains a heavy atom, because its strong spin-orbit interaction can reverse the relative orientations of pairs or electrons. Emission rates are slow and hence fluorescence lifetimes are longer. The fluorescence lifetime, $\tau$, is the average period of time a fluorophore remains in the excited state prior to its return in the ground state [2]

## 3.3 Photophysics of Ruthenium Complex

Luminescence-based sensors have been used to measure oxygen, pH, $CO_2$ and temperature [3, 4, 5, 6, 7, 8, 9]. Luminescent transition metal complexes form an important class of sensor materials and their response is monitored by changes in luminescence intensity (I) or lifetime ($\tau$) [10]. These complexes show strong absorption in the blue region of the spectrum, and have a large Stokes shift. They also have long unquenched lifetimes which are relatively easy to measure [11, 12]. There are many complexes which are suitable for oxygen sensing. A particular complex $[Ru(Ph_2phen)_3]Cl_2$ ($Ph_2phen = 4,7-diphenyl-1,10-phenanthroline$), Ru(dpp), is widely used [11, 12]. This complex has all the above mentioned advantages as well as being thermally, chemically and photochemically robust which makes it particularly suitable for use as a sensor for oxygen [10]. Figure 3.2 shows the structure of the ligand ($Ph_2phen$) which is bound to the ruthenium molecule via nitrogen atoms (N) [13]. Each ruthenium molecule has three of these ligands bound to it.

Transition metal complexes are characterised by partially filled d orbitals. To a considerable extent the ordering and occupancy of these orbitals determine emissive properties [10].

Figure 3.3 shows a simplified energy level diagram for a representative d metal complex. The octahedral crystal field of the ligands splits the four degenerate d orbitals by an amount $\Delta$ into a triply degenerate t level and doubly degenerate e level.

The splitting occurs because the two e orbitals are directed towards the six ligands and the remaining t orbitals point between the ligands, resulting in the e orbitals being higher in energy than the t orbitals. The ligands have $\pi$ and $\sigma$

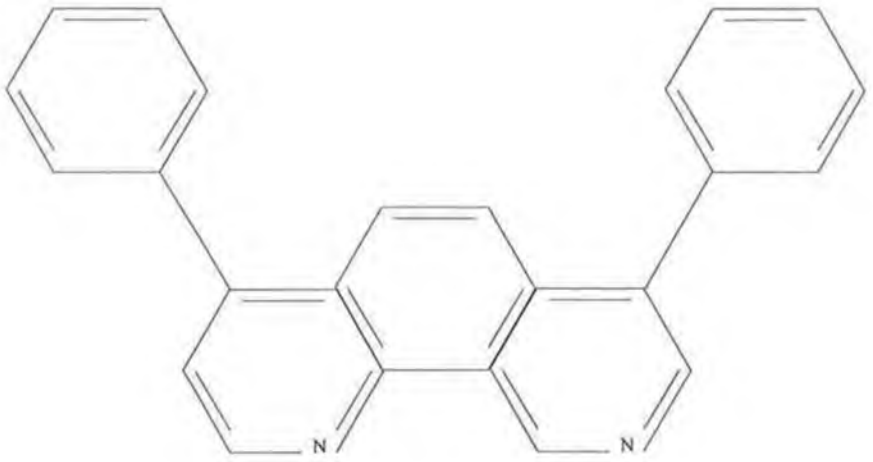


**Figure 3.2:** Chemical structure of 4,7- diphenyl, 1-10-phenanthroline ($Ph_2phen$)

orbitals, but only the $\pi$ orbitals are important for visible and near-uv absorptions and emissions. There are both $\pi$ bonding and $\pi$ antibonding ($\pi^*$) levels and the $\pi$ bonding levels are filled.

There are three types of excited states:

1. Metal-achieved d-d states where a d electron is promoted to another d level.
2. Ligand-based $\pi - \pi^*$ states achieved by promoting an electron from a $\pi$ bonding orbital to a $\pi^*$ antibonding orbital.
3. Charge-transfer states obtained by either promoting a d electron to a $\pi^*$ antibonding (MLCT state) orbital or promoting an electron in a $\pi$ bonding orbital to an unfilled d orbital.

The MLCT (Metal to Ligand Charge-Transfer) states are easiest to pump and are the most stable. They are primarily responsible for the absorption and emission characteristics of the complex.

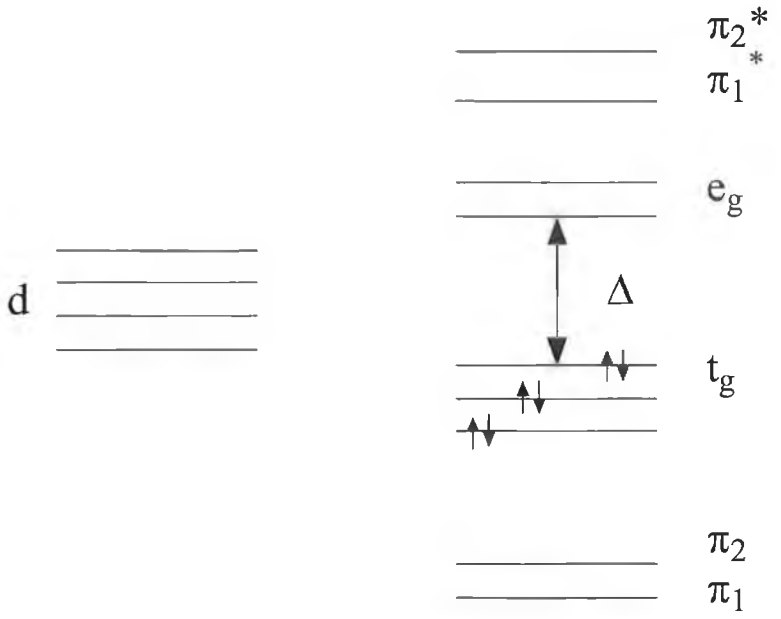


**Figure 3.3:** Simplified energy-level diagram

## 3.4 Stern-Volmer equation and oxygen sensing

Fluorescence quenching is a process by which an excited state is depopulated without the emission of a photon. There are two different types of quenching: static and dynamic.

1. *Static*: occurs when a non-fluorescent ground state complex is formed between the fluorophore and quencher. When this complex absorbs light, it immediately returns to the ground state without the emission of a photon.

2. *Dynamic*: is where quenching is a result of collisional encounters between the quencher and the fluorophore. The quencher must diffuse to the fluorophore during the lifetime of the excited state. Upon contact, the fluorophore returns to the ground state without the emission of a photon. In this work dynamic quenching is the quenching mechanism.

When an oxygen molecule collides with a fluorophore in an excited state a very short-lived (ns) oxciplex is formed, which returns to the ground state without the

emission of a photon. The oxygen dissociates and is therefore not consumed in the process. The intensity and lifetime of the fluorophore are affected by the concentration of oxygen. Both decrease with the increasing quencher concentration.

The quenching process is described by the Stern-Volmer equation [14].

$$I_0/I = 1 + K_{SV}[pO_2] \tag{3.1}$$

$$K_{SV} = k\tau_0 \tag{3.2}$$

where $I_0$ and $\tau_0$ are, respectively, the fluorescence intensity and excited state lifetime in the absence of oxygen. I is the intensity at a given partial pressure of oxygen, $pO_2$, $K_{SV}$ is the Stern-Volmer coefficient and k is the bi molecular quenching constant.

The Stern-Volmer equation can also be expressed in terms of the lifetime, $\tau$, of the fluorophore, where the lifetime is seen to decrease with an increase in oxygen concentration:

$$\tau_0/\tau = 1 + K_{SV}[pO_2] \tag{3.3}$$

It is also important to note that the following relationships are also relevant to the quenching process.

$$k \propto P = SD \tag{3.4}$$

i.e. k is proportional to permeability, P, which is given by the product of the solubility, S, and diffusion coefficient, D.

Oxygen solubility, S, obeys Henry's Law at low pressures. The mass of gas dissolved is related to the free volume in the sol-gel matrix. Recent studies on hydrophobic polymer films highlight the very small variation in oxygen solubility across a range of films [15].

Pauly et al. [16] showed that the higher the oxygen permeability the greater the oxygen sensitivity of the film. From Equation 3.4 it can be seen that permeability, P, is directly related to solubility, S, and diffusion coefficient, D. As already noted, oxygen solubility does not vary much between different sol-gel films. Therefore it is thought that the variation of D dominates the observed variation in sol-gel medium permeability and therefore dominates the sensitivity of the oxygen sensitive film.

The porosity of the matrix also plays an important role in determining both the sensitivity and response time of optical sensors. For gas sensors, the diffusion coefficient for the analyte gas through the matrix increases with film porosity. This in turn increases the sensitivity of the sensor response via the Stern-Volmer coefficient.

The volume fraction porosity, $V_p$,is that fraction of the total volume of the film which is occupied by empty pores. This is related to the total surface area of the pores, $A_p$, by:

$$V_p = R_h \times A_p \tag{3.5}$$

where $R_h$ is the hydraulic radius or the average pore radius [17]. For an analyte diffusing through the film, the permeability, P, is given by:

$$P = (1 - \rho)\frac{R_h^2}{f_s f_t} \tag{3.6}$$

where $\rho$ is the relative density of the film and $f_s$ and $f_t$ are factors which account for the shape of the pores and the nonlinear path in real materials [17].

In general, an increase in film porosity is related to an increase in average pore radius. From Equations 3.4 and 3.6, the analyte diffusion coefficient, D, is proportional to the square of the average pore radius, leading to the conclusion, from Equation 3.5, that an increase in film porosity is indicative of a higher diffusion coefficient in the material assuming a constant solubility.

Another form of the Stern-Volmer equation used by Liu et al. [18] to describe oxygen quenching of phosphorescence under steady-state illumination is given by the following expression:

$$I_0/I = (1 + \pi g R N D[O_2]\tau_0/1000)(X/Y) \tag{3.7}$$

where, as before, $I_0$ is the intensity in the absence of oxygen and I is the intensity at a given oxygen concentration $[O_2]$. The spin statistical factor associated with the quenching of triplets by oxygen is given by g. R is the effective phosphor-oxygen quenching encounter distance. N is Avogadro's number and D is the oxygen diffusion coefficient. The term X allows for the possibility of static quenching by oxygen molecules while Y is a transient diffusional term allowing for the time required to establish steady state. Under quenching conditions, X and Y are close to unity and can be neglected as a good approximation [18]. For oxygen quenching of triplets, a

spin statistical factor of $\frac{1}{9}$ for g is suitable [19], while a value of $1 \times 10^{-7}$ is suitable for R [20]. At room temperature, $[O_2] = (.041)(S)(p_{ox})$ where S is the oxygen solubility and $p_{ox}$ is the oxygen partial pressure in atmospheres. Substitution of all these changes into Equation 3.7, produces the following Equation:

$$I_0/I = 1 + 3.4 \times 10^{12} P_{ox} \tau_0 p_{ox} \tag{3.8}$$

Therefore

$$K_{SV} = 3.4 \times 10^{12} SD\tau_0 \tag{3.9}$$

Quenching data is often presented as a plot of $I_0/I$ verus p$O_2$, as seen in Figure 3.1. The Stern-Volmer should yield a straight line with a y-intercept of 1 and a slope equal to $K_{SV}$. Usually optical oxygen sensors show a downward curving Stern-Volmer line graph as seen from Figure 3.4.

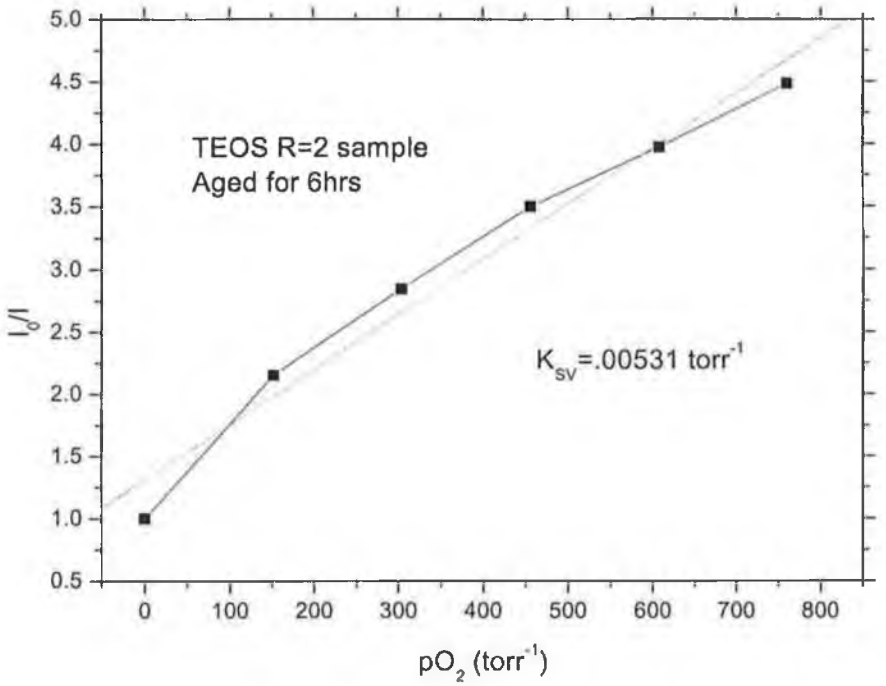


**Figure 3.4:** A typical Stern-Volmer graph for a TEOS R=2 sol-gel sample

The downward curving Stern-Volmer graph is attributed to a multitude of quenching sites within the same sensing film, each site having its own Stern-Volmer constant [15].

## 3.5 Diffusion in sol-gel films

### 3.5.1 Introduction

As already mentioned in Section 3.4, the fluorescence from doped sol-gel films used in this work is quenched in the presence of oxygen. This quenching process is described using the Stern-Volmer equation (Equation 3.1). The greater the permeability, the greater the oxygen sensitivity of the film. However from Equation 3.4, it can be seen that P depends on solubility and the diffusion coefficient. Solubility does not vary much from film to film, because it is the variation of D that dominates the sensitivity of the oxygen sensitive films.

To expand on this, if the forward and reverse rates of interaction between the analyte and the sensor dye are very rapid, then it is likely that the response and recovery times of an oxygen sol-gel-derived sensor will be decided by the rate of diffusion into and out of the sensor film, respectively, and this situation can readily be modelled.

### 3.5.2 Development of the diffusion model

Diffusion is considered a random process whereby matter is transported through a system by a series of random molecular motions [21]. The mathematical model used to describe diffusion is know as Fick's first law [21]. It is based on the hypothesis that the rate of transfer of a diffusing species through a unit area of section is proportional to the concentration gradient measured normal to that section and is given by the following expression:

$$F = -D\frac{\partial C}{\partial x} \tag{3.10}$$

where F is the rate of transfer per unit area of section, C is the concentration of diffusing substance, x is the space coordinate measured normal to the section, and D is called the diffusion coefficient.

Fick's second law, can be derived from Fick's first law and is given by [21]:

$$\frac{\partial C}{\partial t} = D\frac{\partial^2 C}{\partial x^2} \tag{3.11}$$

In the model used in this work, the optical sensor film is considered to be in the form of a plane sheet of thickness, $l$. The analyte diffusion coefficient is D. At x=0,

the film interfaces with a gas-impermeable medium such as glass. The concentration at x=0 is set at $c_1$. At x=$l$, the film interfaces with a medium of infinite volume that contains the analyte under test. At x=$l$ the concentration is set at $c_2$.

Therefore the initial conditions of the model are as follows:

$$C = c_1, \quad x = 0, \quad t \geq 0, \tag{3.12}$$

$$C = c_2, \quad x = l, \quad t \geq 0, \tag{3.13}$$

$$C = f(x), \quad 0 < x > l, \quad t = 0, \tag{3.14}$$

Therefore using Fick's second law, (Equation 3.11), and the above conditions hold, the concentration distribution within the film due to diffusion of the analyte into the film will be described by the following expression [21]:

$$\Psi(\gamma, \chi) = \frac{c_{\gamma,\chi} - c_1}{c_2 - c_1} \tag{3.15}$$

$$= 1 - 4\pi^{-1} \sum_{n=0}^{\infty} (-1)^n \theta^{-1} exp\left(\frac{-\theta^2 \pi^2 \gamma}{4}\right) cos\left(\frac{\theta \pi \chi}{2}\right) \tag{3.16}$$

where $\gamma$ (a normalised time parameter)=$Dt/l^2$, $\theta$=(2n+1) and $\chi = x/l$ (a normalised thickness parameter). The parameter $c_{\gamma,\chi}$, is the concentration of the analyte , at distance $\chi$ from the gas impermeable membrane but still within the film, and at time $\gamma$ after the concentration was first changed from $c_1$ to $c_2$.

In measuring the response and recovery times for an optical sensor, it is usually taken that response times refer to an increase in analyte concentration, i.e. $c_1 \longrightarrow c_2$, with $c_2 > c_1$. Recovery times refer to the reverse process, i.e., $c_2 \longrightarrow c_1$. In this case, the concentration distribution within the film as a function of time following the change from $c_1$ to $c_2$ will be described by the expression:

$$\Psi'(\gamma, \chi) = \frac{c_{\gamma,\chi} - c_1}{c_2 - c_1} \tag{3.17}$$

$$= 4\pi^{-1} \sum_{n=0}^{\infty} (-1)^n \theta^{-1} exp\left(\frac{-\theta^2 \pi^2 \gamma}{4}\right) cos\left(\frac{\theta \pi \chi}{2}\right) \tag{3.18}$$

Sol-gel based optical oxygen sensors exhibit an asymmetrical response-recovery behavior with a hyperbolic-type response. Meaning that when the response-recovery fluorescence intensities are plotted with respect to time, the curve is similar to a hyperbolic-type curve. Also the response times appear to decrease and the recovery times appear to increase the larger the change in analyte concentration [22].

When the concentration is changed from $c_1 \longrightarrow c_2$ the optical signal (I) is seen to decrease. Similarly, for the reverse process $c_2 \longrightarrow c_1$, the signal (I) increases. It is usual to represent response and recovery times with respect to an overall fractional change in the signal. In this work the measured response times were characterised by $t_{90}$ or the time taken to achieve 90% of the optical signal change.

In the model developed in this project the fractional change in the optical signal is given by the expression [15]:

$$\frac{I_{\gamma,\chi} - I_2}{I_1 - I_2} \tag{3.19}$$

where $I_{\gamma,\chi}$ is the average signal associated with the film at time $\gamma$. $I_1$ is the signal when the concentration is equal to $c_1$ and $I_2$ is the signal at concentration $c_2$.

From Equations 3.16 and 3.19 [22], the following expression can be derived, showing the fractional optical signal change due to diffusion:

$$\frac{I_{\gamma,\chi} - I_2}{I_1 - I_2} = \frac{1 + K_{SV}c_2}{1 + K_{SV}c_{\gamma,\chi}} \times \Psi(\gamma,\chi) \tag{3.20}$$

But $c_1$=0, and therefore it follows from Equation 3.16 that $c_{\gamma,\chi}$=$K_{SV}c_2\Psi(\gamma,\chi)$. Thus the optical signal distribution within the film due to diffusion into the film is given by the expression:

$$\frac{I_{\gamma,\chi} - I_2}{I_1 - I_2} = \frac{\Psi'(\gamma,\chi)}{1 + c^*\Psi(\gamma,\chi)} \tag{3.21}$$

where the expression $c^* = K_{SV} \times c_2$, and $\Psi(\gamma,\chi)$ and $\Psi'(\gamma,\chi)$ are defined in Equations 3.16 and 3.18.

Similarly it can be shown that the change in the optical signal due to diffusion out of the film is given by:

$$\frac{I_{\gamma,\chi} - I_2}{I_1 - I_2} = \frac{\Psi(\gamma,\chi)}{1 + c^*\Psi'(\gamma,\chi)} \tag{3.22}$$

Therefore it is possible to calculate the signal distribution within the film as a

function of $\gamma$ and $\chi$ for a given value of $c^*$ using the functions given in Equations 3.21 and 3.22.

To best show how this model is capable of calculating numerically the diffusion coefficient, actual experimental data is used in the description below.

Plots of the average fractional change of the optical signal as a function of $\gamma$ for different values of $c^*$, due respectively to the diffusion of an analyte into and out of a plane sheet, are shown in Figures 3.5 and 3.6. The thickness of the film investigated was 499nm as measured using profilmetry. The data for the graphs were compiled using the computer program in Appendix A.

The plots shown in Figures 3.5 and 3.6 show the asymmetrical response-recovery behavior of optical sensors where response times prove to be shorter than recovery times and the shape of the graphs follow that of a hyperbolic curve. The effect of the change of concentration is also noted where an increase in $c^*$ ($c^*$ is directly related to concentration, $c_2$) results in shorter response times and longer recovery times.

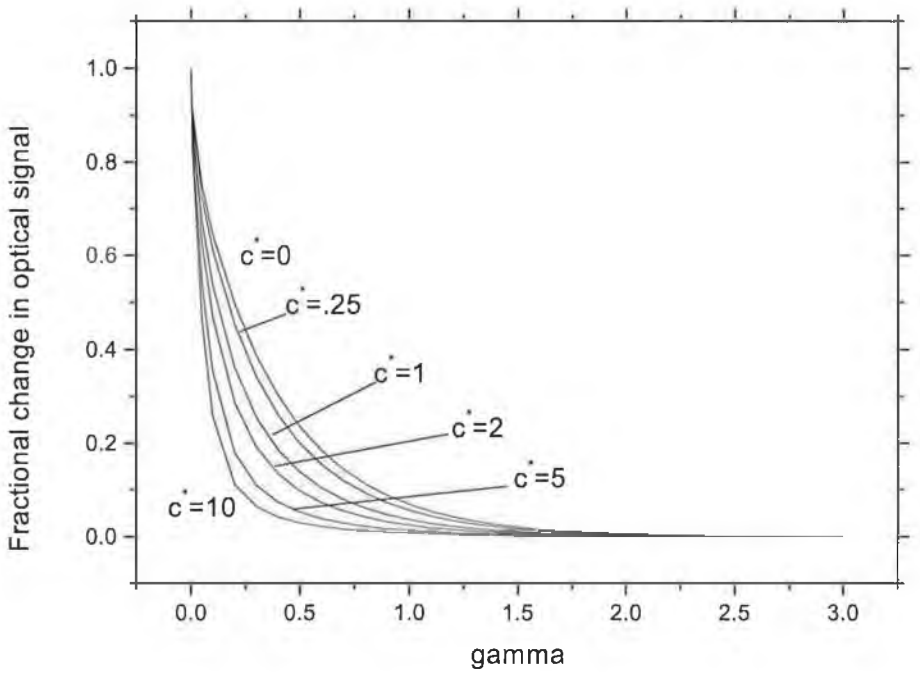


**Figure 3.5:** Plot of the average fractional change in the optical signal as a function of $\gamma$ due to diffusion of an analyte into a film

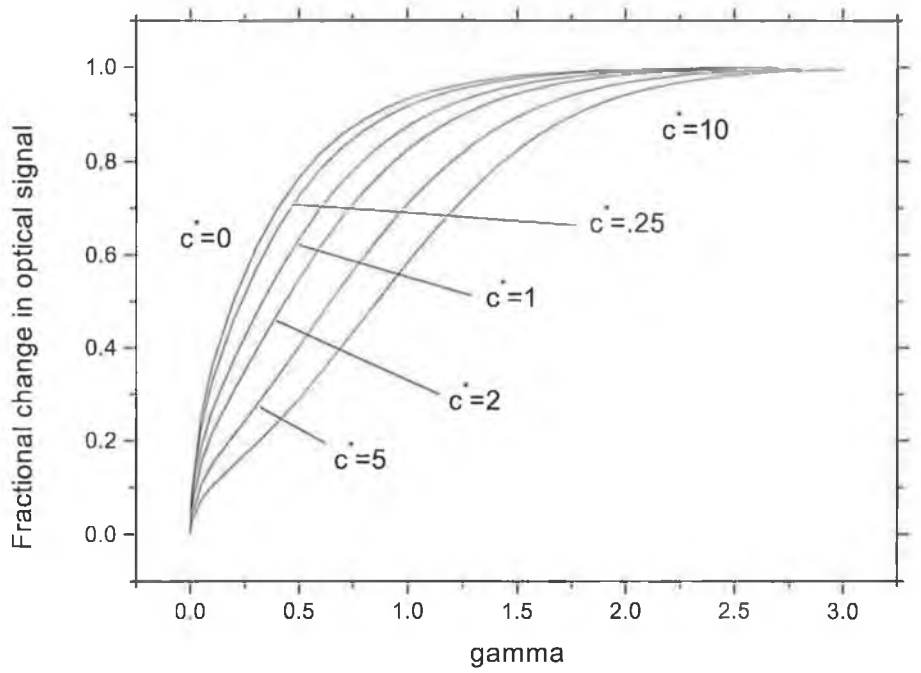


**Figure 3.6:** Plots of the average fractional change in the optical signal as a function of $\gamma$ due to diffusion of an analyte out of a film

### 3.5.3 Application of the diffusion model

When calculating the diffusion coefficient of a sample, a number of factors must be known. These include the thickness, $l$, of the sample along with $t_{90}\uparrow$ (recovery time) and $t_{90}\downarrow$ (response time). The following is an important assumption that is made in the model.

$$\frac{\gamma_{90}\uparrow}{\gamma_{90}\downarrow} = \frac{t_{90}\uparrow}{t_{90}\downarrow} \tag{3.23}$$

where $\gamma_{90}\uparrow$ and $\gamma_{90}\downarrow$ are the recovery and response times for the normalised time parameters and $\gamma{=}Dt/l^2$. Plots similar to Figure 3.5 were calculated for a range of different $c^*$ values. As can be seen for each value of $c^*$, there are corresponding values of $\gamma_{90}\uparrow$ and $\gamma_{90}\downarrow$. Therefore for a given thickness, $l$, it is possible to determine $\gamma_{90}\uparrow/\gamma_{90}\downarrow$ as a function of $c^*$ as can be seen from Figure 3.7

Since $t_{90}\uparrow/t_{90}\downarrow$ is known, a corresponding $\gamma_{90}\uparrow/\gamma_{90}\downarrow$ can be calculated using Equation 3.23. Using the calculated value of $\gamma_{90}\uparrow/\gamma_{90}\downarrow$ a value of $c^*$ can be calculated using Figure 3.7. The model is now used again using this calculated value of $c^*$ to return values of $\gamma_{90}\uparrow$ and $\gamma_{90}\downarrow$. The diffusion coefficient, D, can then

be calculated from the expression $\gamma = Dt/l^2$.

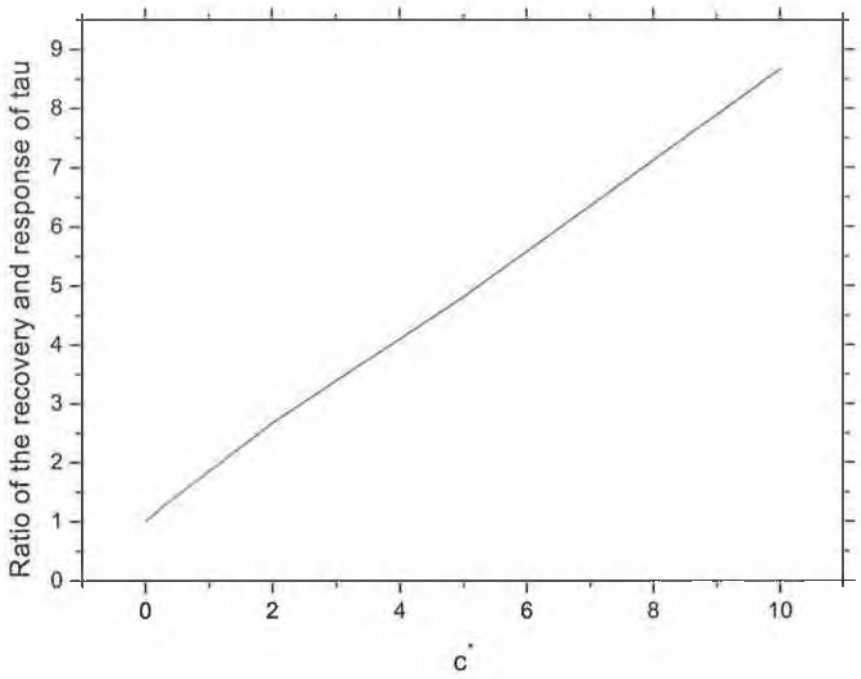


**Figure 3.7:** Plot of the ratio of $\gamma_{90} \uparrow / \gamma_{90} \downarrow$ verus $c^*$ calculated using the model generated data from Figure 3.5

For example consider the film of thickness 499nm. The measured response and recovery times are 40.2 and 103ms respectively. Therefore using Equation 3.23:

$$\frac{\gamma_{90} \uparrow}{\gamma_{90} \downarrow} = \frac{t_{90} \uparrow}{t_{90} \downarrow} = \frac{103}{40.2} = 2.56 \tag{3.24}$$

From Figure 3.7 a value of $\gamma_{90} \uparrow / \gamma_{90} \downarrow$=2.56 has a corresponding $c^*$ value of 1.84. Running the computer program using this particular value of $c^*$ gives a $\gamma_{90} \downarrow$ equal to 0.52. But $\gamma = Dt/l^2$. Following on from this:

$$\gamma = 0.52 = \frac{D40.2 \times 10^{-3}}{(499 \times 10^{-9})^2} \tag{3.25}$$

and

$$D = 3.2 \times 10^{-12} m^2 s^{-1} = 3.2 \times 10^{-8} cm^2 s^{-1} \tag{3.26}$$

The diffusing coefficient calculated above uses the response time. When the recovery time was used instead, it resulted in a diffusion coefficient of $3.17 \times 10^{-8} cm^2 s^{-1}$.

## 3.6 Conclusion

This chapter introduced the fundamentals of oxygen sensing and the reasons for using ruthenium complexes in optical sensing have been outlined.

The Stern-Volmer equation is introduced and it is shown how it can be used to characterise a sensing film. Factors affecting the sensitivity of a film, namely, permeability, diffusion coefficient, Stern-Volmer coefficient and solubility, were introduced.

An increase in porosity was shown to lead to a higher diffusion coefficient. This in turn, leads to a greater film permeability and higher oxygen sensitivity. To investigate further the effect of diffusion on the behavior of a sol-gel film, a numerical model was developed to calculate the diffusion coefficients. This model is successful in showing the asymmetrical response-recovery behavior of optical sensors with a hyperbolic-type of response as well as enabling the calculation of diffusion coefficients for the sol-gel derived oxygen sensitive films.

# Bibliography


[1] A. Gilbert and J. Baggot. *Essentials of Molecular Photochemistry.* Blackwell Scientific Publications, Oxford, 1991.

[2] G.D. Christian. *Analytical Chemistry.* Wiley, New York, 1971.

[3] J.R. Bacon, E.R. Carraway, J.N. Demas, and B.A. DeGraff. Photophysics and photochemistry of oxygen sensors based on luminescent transition-metal complexes. *Analytical Chemistry*, 63:337–342, 1991.

[4] R.A. Povtyrailo and G.M. Hieftje. Oxygen detection by fluoresence quenching of tetraphenylporphyrin immobilised in the orginal cladding of an optic fibre. *Analytica Chimica Acta*, 370:1–8, 1998.

[5] S.B. Bambot, R. Holavanahali, J.R. Lakowicz, G.M. Carter, and G. Rao. Phase fluorometric sterilizable optical oxygen sesnor. *Biotechnology and Bioengineering*, 43:1139–1145, 1994.

[6] B.D. MacCraith, C.M. McDonagh, G. O'Keefe, A.K. McEvoy, T. Butler, and F.R. Sheridan. Sol-gel coatings for optical chemical sensors and biosensors. *Sensirs and Actuators B*, 29:51–57, 1995.

[7] S.A. Degraff, Wenying Xu, R.C. McDonough, B. Langsdorf, and J.N. Demas. Oxygen sensors based on luminescence quenching: Interactions of metal complexes with the polymer supports. *Analytical Chemistry.*, 66(23):4133, 1994.

[8] W. Xu, R. Schmidt, M. Whaley, J.N. Demas, B.A. DeGraff, E.K. Karikari, and B.L. Farmer. Oxygen sensors based on luminescence quenching: Interactions of pyrene with the polymer supports. *Analytical Chemistry*, 67(18):3172–3180, 1995.

[9] O. Worsfold, C. Malins, M.G. Forkan, I.R. Peterson, B.D. MacCraith, and D.J. Walton. Optical NO2 sensing based on sol-gel entrapped azobenzene dyes. *Sensors and Actuators B-Chemical*, 56(1-2):15–21, 1999. JUN 1 SENSOR ACTUATOR B-CHEM.

[10] J.N. Demas and B. A. DeGraff. Design and applications of highly luminescent transition metal complexes. *Analytical Chemistry*, 63:829A–837A, 1991.

[11] B.D. MacCraith, C. McDonagh, G. O'Keeffe, E.T. Keyes, J.G. Vos, B. O'Kelly, and J.F. McGilp. Fibre optic oxygen sensor based on fluorescence quenching of evanescent-wave excited ruthenium complexes in sol-gel derived porous coatings. *Analyst*, 118:385–388, 1993.

[12] W. Xu, R.C. MacDonagh, B. Langsdorf, J.N. Demas, and B.A. DeGraff. Oxygen sensors based on luminescence quenching: Interactions of metal complexes with the polymer supports. *Analytical Chemistry*, 66:4133–4141, 1994.

[13] F. Sheridan. *Characterisation and optimisation of sol-gel derived thin films in optical sensing.* Master of science, Dublin City University, 1995.

[14] O. Stern and M. Volmer. *M. Phys. Z*, 20:183, 1919.

[15] A. Mills. Controlling the sensitivity of optical oxygen sensors. *Sensors and Actuators B*, 51:60–68, (1998).

[16] S. Pauly. *Polymer Handbook VI.* Wiley, New York, 1989.

[17] C. Jeffrey Brinker and George W. Scherer. *Sol-Gel Science.* Academic Press Inc., San Diego, 1990.

[18] H.Y. Liu, S.C. Switalski, B.K. Coltrain, and P.B. Merkel. Oxygen permeability of sol-gel coatings. *Applied Spectroscopy*, 46(8):1266–1272, 1992.

[19] D.R. Kearns. Physical and chemical properties os singlet molecular oxygen. *Chemical Review*, 71:395–427, 1971.

[20] P.F. Jones and S.Siegal. Quenching of naphthalene luminescence by oxygen and nitric oxide. *Journal of Chemical Physics*, 54:3360–3366, 1971.

[21] J. Crank. *The Mathematics of Diffusion.* Claredon Press, Oxford, 1956.

[22] A. Mills and Q. Chang. Controlling the sensitivity of optical oxygen sensors. *Analyst*, 117:1461–1466, 1992.

# Chapter 4

# Experimental Techniques

## 4.1 Introduction

This chapter details the fabrication of a wide range of sol-gel-based films. These include TEOS, MTEOS, phenyl-substituted silica as well as soluble ormosil films.

As already mentioned, the sol-gel process is very well adapted for thin film formation, and the process parameters can be controlled to provide a microporous support matrix in which analyte-sensitive species are entrapped, allowing easy access by analyte molecules.

Because the porosity of the matrix plays an important role in determining response time and sensitivity of the optical sensor, an experimental procedure used to measure porosity of sol-gel thin films was developed.

The average pore size in the sol-gel films investigated in this work is between 3 and 9Å approximately, making it very difficult to accurately measure the porosity [1]. A technique was developed to measure the porosity of a sol-gel film , incorporating an ellipsometer and a specially-designed gas cell [2] and applying a form of the Lorentz-Lorenz equation. A number of different films were fabricated using different tailoring techniques for the purpose of controlling porosity. The porosity of these films was measured using the described technique. Porosity measurements were correlated with previous data for the tailoring of films.

The response time for surface-adsorbed luminescent oxygen sensor has been reported to be as fast as 5ms for a 90% signal change (i.e. $t_{90}$) [3]. In measuring the true response time of a gas sensor, the gas exchange times of the measurement chamber (including gas cell and gas lines) have to be minimised as this exchange

time normally masks the underlying intrinsic sensor response time.

Therefore, measurements of sensor response times shorter than previously reported require the generation of fast (submillisecond) pressure changes. By incorporating the sol-gel oxygen sensitive film inside a solenoid valve, a submillisecond pressure jump was created from a vacuum to an environment of $O_2$ at atmospheric pressure. An optical detection system was used to illuminate the sol-gel sample and collect the resultant fluorescence. The signal from the photodiode was collected by a data acquisition card and processed using a Labview program. The solenoid valve used to switch from a vacuum to a $N_2$ environment was also under the control of a Labview program. The response times of a range of films was measured using this system. The experimental apparatus developed for this work is described in detail in this chapter.

Some of the other equipment used over the course of the work such as the Dektak profilmeter, Metricon prism coupler and the Cahn contact angle analyser are also detailed.

## 4.2 Film fabrication of TEOS and MTEOS films

### 4.2.1 Sol preparation

Sols were prepared using the precursors tetraethoxysilane (TEOS) and methyltriethoxysilane (MTEOS). The ruthenium complex was synthesised and purified as described in the literature [4]. The correct amount of ruthenium complex, 20,000 parts per million [5] (weight of ruthenium complex relative to the amount of silica), to fabricate a sol was first added to a vial. Then volumes of water, acid and ethanol were added and stirred for a period of time. The correct volume of precursor was then added dropwise to the solution to ensure complete mixing. The sols were then left to stir for 2 hours before aging. However the MTEOS-based sols were not aged but dip-coated onto suitable substrate such as glass or silicon slides and then dried. The MTEOS-based sols were not aged because of the high rates at which hydrolysis and polycondensation occur and elevated temperatures would lead to subsequent gelation of the sol after a short period of time.

During aging, the vial containing the TEOS-sol is sealed to prevent fast evaporation and subsequent gelation, but a tiny hole in the lid of the vial allows for slow evaporation and pressure release . Aging occurs in an oven at 70°C for the required

period of time. After aging, the sol is sufficiently viscous to dip-coat planar substrates, the withdrawal speed determining the film thickness. As seen in Chapter 3, a faster withdrawal speed gives a thicker coating (Equation 2.1). The dip-coating apparatus will be shown in greater detail later in this chapter. Having coated the substrates, they are dried at 70°C for approximately 18 hours. In the following sections, the fabrication techniques used will be described in detail.

### 4.2.2 Film fabrication techniques

#### 4.2.2.1 Water:precursor ratio (R-value)

As described in Section 2.3.1, the R-value plays a vital role in the structure and characteristics of the sol-gel film. Sols were prepared using R-values of 2 and 4, and the precursors used were TEOS and MTEOS. When preparing MTEOS and TEOS films, the catalyst used was HCl at pH1. After the correct volumes of precursor, ethanol, water and HCl were mixed together, the mixture was left to stir for 2 hours. TEOS-based films were then aged for specific periods of time prior to dipping onto suitable substrates and then dried. No aging was carried out on MTEOS samples due to the fast rate at which hydrolysis and condensation occur. After stirring, the MTEOS sol-gel was dip-coated onto suitable silicon or glass slide substrates and then dried.

#### 4.2.2.2 Ethanol:TEOS ratio

In order to examine the effect of varying the ethanol concentration, films were prepared using TEOS, HCl and varying amounts of ethanol. The ethanol:TEOS value was varied using values of 1.5, 2 and 3. The R-value was equal to 4 and the catalyst used was HCl at pH1 . The precursor used was TEOS. The aging time for the sol was 6 hours. The aging time was kept short because of the very short gelling times associated with high ethanol content. Dip-coating was then carried out and the films were dried in the manner already described.

#### 4.2.2.3 pH of catalyst

In order to examine the effect of varying pH, films were prepared using TEOS, ethanol and HCl of varying pH. The pH of the catalyst was varied between pH1 and 4. The precursor was TEOS and the R-value was 4. At pH4 the aging time was

varied between 4 and 6 hours followed by dip-coating and drying of the films. As with varying the ethanol:TEOS ratio, the aging times were short due to fast gelation times associated with sols fabricated using a catalyst at pH4.

#### 4.2.2.4 Aging time

When preparing films to investigate the sole effect of aging time, the films were prepared using the precursor, TEOS. The R-values investigated were 2 and 4. The aging times investigated were as follows: 2, 4, 6, 8 and 16 hours. The pH of the catalyst used was 1 and the ethanol:TEOS ratio was 3. After aging, the sol was allowed to reach ambient temperatures and it was then ready to be used in the dip-coating process.

## 4.3 Fabrication of phenyl-substituted silica films

Phenyl-substituted silica films are of interest because by changing the quantities of the phenyl- and methyl-modified precursors in the sol-gel mixture, the refractive index can be varied and controlled while keeping the organic fraction of the material constant. This leads to the possibility of using oxygen sensitive phenyl-substituted silica in waveguides or to incorporate the phenyl substituted silica into a silica-based integrated optical circuit [6].

The starting materials were methyltriethoxysilane (MTEOS), phenyltriethoxysilane (PhTEOS), methyltrimethoxysilane (MTMOS) and tetraethoxysilane (TEOS). The precursor:water ratio (R-value) was equal to 4. The sol-gel was prepared by first mixing the three precursors PhTEOS, MTEOS and TEOS together, and then stirring for approximately 15 minutes in a vial containing 15mg of the oxygen sensitive dye, Ru(dpp). The correct volume of water was then added dropwise, HCl acid at pH1. At this point, the mixture was observed to grow cloudy. After a period of approximately 10-30 minutes the sol changed from a cloudy to a dark orange colour and the vial containing the sol was hot to touch, indicating an exothermic reaction. The sol was left to stir for approximately 24 hours. The samples were then dip-coated at 3mm/s and dried at 70°C for 18 hours.

A number of different films were fabricated by mixing the three precursors together in different ratios. The various films created were designated by the mole fraction of the three precursors. For example, a film designated 30/50/20 indicates

a film prepared using the molar ratio 30:50:20 for MTEOS/PhTEOS/TEOS. In general, samples were prepared using the molar ratios MTEOS/PhTEOS/TEOS =x/(80-x)/20 and x/(60-x)/40. Samples containing the precursors MTMOS, PhTEOS and TEOS were prepared in an identical manner as described above.

In addition to films fabricated using three precursors, films were prepared using two precursors, namely PhTEOS mixed with TEOS or MTEOS. As before the precursor:water ratio was 4 using the catalyst HCl at pH1 . The precursors were added together using the ratios x/(100-x). Prior to dipping at 3mm/s, the sol was left to stir for 24 hours. The films were then dried at 70°C for 18 hours.

## 4.4 Fabrication of other film types incorporating Ru(dpp) into the film matrix

### 4.4.1 Soluble ormosils

An additional support matrix that was investigated for the entrapment of Ru(dpp) was a hybrid matrix known as a soluble ormosil. Soluble ormosils combine the features of both polymer and sol-gel based films. They are soluble in organic solvents like polymers, and are mechanically stable like sol-gel based films. These materials are also hydrophobic making them suitable for dissolved oxygen sensing [5, 7]. The main advantage of these materials with respect to this work is their sol-gel like porous structure, that allows them to be doped with indicator dyes.

Films were prepared by dissolving 0.5g of the ormosil and 3.5mg of ruthenium complex in 25ml of chloroform [7]. The mixture was allowed to stir for 1 hour. Glass slides were then dip-coated at a speed of 3mm/s, and the coated glass slides were dried at 70°C for 18 hours.

### 4.4.2 Films fabricated with MTEOS and TEOS mixed together in different molar ratios

Films were prepared using the precursors MTEOS and TEOS mixed together in the molar ratios of MTEOS:TEOS = 2, 3 and 4:1 with the correct mass of Ru(dpp). The precursor:water ratio (R-value) was 4 and the catalyst was HCl at pH1. The sol was left to stir for 24 hours prior to dipping at 3mm/s, after which the slides

were dried at 70°C for 18 hours.

## 4.5 Substrate preparation

It is important to ensure that before a sol-gel is coated onto a substrate that the surface of the substrate is clean and free from dirt. The substrates used were glass microscope slides and silicon slides cut to sizes of approximately 14x30mm. The slides were prepared by washing them in deionised water, methanol and acetone [8]. The slides were then conditioned in deionised water for 24 hours at 70°C, as this is thought to increase the number of surface silanol groups which enhances adhesion of the sol-gel film to the substrate.

## 4.6 Dip-Coating procedure

The theory of dip-coating is described in Section 2.4. In this section the practical aspect is outlined briefly. The dip-coater consists of a movable stage controlled by a computer controlled stepper motor. The sol is held in a vial on the stage which is moved upwards to immerse the substrate as seen from Figure 4.1.

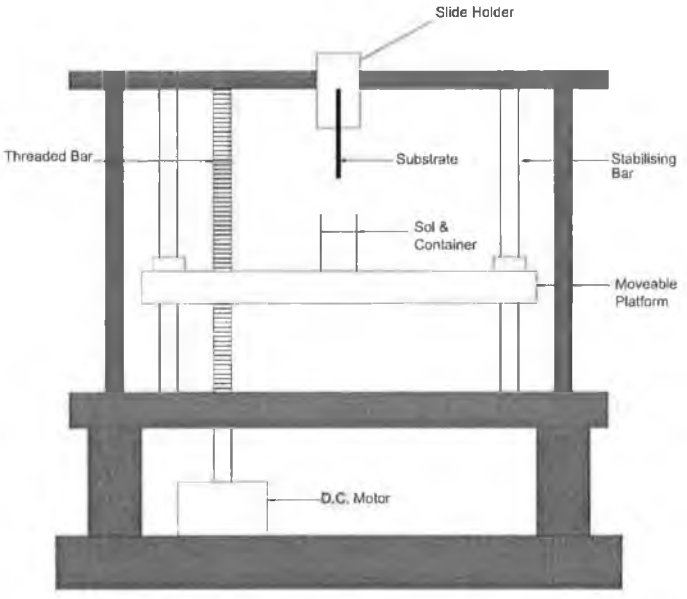


**Figure 4.1:** Dip-coating apparatus

It is then withdrawn at a constant speed. The withdrawal speed of the stage is adjusted by the user and hence the resulting thickness of the film can be controlled

[9]. A perspex hood acts as a draught guard, and vibration dampers are incorporated into the dip-coating apparatus to ensure good film quality. Before dip-coating, the temperature of the sol was left to reach ambient temperature. After dip-coating the slides were dried at 70°C for approximately 18 hours.

## 4.7 Experimental procedure to measure porosity of sol-gel thin films

### 4.7.1 Introduction

To obtain a direct indication of the porosity of a sol-gel film a technique of 'molecular probing' using ellipsometry as the measurement technique was developed [2]. This is accomplished by measuring the change in refractive index of the sol-gel film as dry $N_2$ is flowed over the film. By using the resultant refractive index of the film and applying the Lorentz-Lorenz equation a value for the porosity of the sol-gel film can be calculated.

### 4.7.2 Ellipsometry

The first step in measuring the porosity, $V_p$, of a sol-gel sample is refractive index measurement. These measurements were performed on a Rudolph Auto EL III ellipsometer. Ellipsometry is a technique for the contact-less and non-destructive optical characterisation of films. It is based on the fact that a monochromatic wave changes its state of polarisation when it strikes a non-perpendicular surface. In measuring that change, the software of the ellipsometer can return values of thickness and refractive index. The ellipsometer consists of a laser, polariser, analyser, compensator and detector as seen from Figure 4.2.

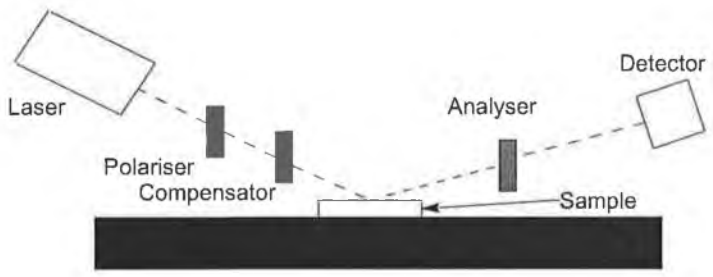


**Figure 4.2:** Schematic diagram of a ellipsometer

The laser is a helium-neon laser at $\lambda$=633nm. The compensator is held at a fixed angle about the optical axis with respect to the plane of incidence. The incident beam and the reflected beam axis is set to 70° relative to the axis. The polariser and analyser, usually high quality prisms, are rotated alternately until the intensity of the beam on the detector is at a minimum. Then the angles of the polariser and analyser with respect to the polarising axis are measured and converted to parameters $\Delta$ and $\Psi$ [10]. The parameters $\Delta$ and $\Psi$ are a function of the incident and reflected light, as well as the real and imaginary refractive indices and thickness of the substrate. Since some of these parameters are already known, the software is able to return values for the thickness and refractive index of the substrate. The thickness is not the true thickness of the substrate but is given by the value of: thickness+m(ordinate), where m is some unknown integer. In this project true thickness was determined using a Metricon profilmeter.

### 4.7.3 Design of the gas cell

The function of the gas cell was to enable control of the gas environment during measurement of the sol-gel film properties with the ellipsometer.

The laser light entering and leaving the gas cell passed through glass windows. The light had to pass through perpendicularly, to maximise transmission through the glass. The windows used also had to introduce minimum birefringence to the system to eliminate any change in the state of the polarisation of the light. Birefringence can be described as the dependence of the refractive index on the orientation of the E-field with respect to the optic axis [11]. Since the ellipsometer is based on making measurements on polarisation variations, if the state of polarisation of the laser changed when passing through the glass, errors would be introduced.

### 4.7.4 Experimental procedure

Figure 4.3 shows the experimental set-up used to make a porosity measurement. The first step in measuring the porosity, $V_p$, of a sol-gel sample is refractive index measurement. These measurements were performed on a Rudolph Auto EL III ellipsometer. The sample to be investigated was placed in the specially designed gas cell. The gas cell was then placed on the sample table of the ellipsometer as seen from Figure 4.3. Dry $N_2$ gas was then flowed through the gas cell, ensuring

that all physisorbed water was removed from the pores. This had the effect of emptying the pore structure of the sol-gel matrix [12]. However it will not remove chemisorbed water. The fabrication of the sol-gel thin films requires a drying regime at $70^0$C. This low temperature will not drive off the chemisorbed water that lies within the pore structure of the sol-gel thin film. However the type of film involved (hydrophobic/hydrophilic) will influence the amount of chemisorbed water present. This factor plays a vital role in the oxygen sensitivity of sol-gel films and will be discussed in more detail in later chapters. During this period of time when dry $N_2$ was flowing through the gas cell, the refractive index was seen to decrease. The gas was allowed to flow until the refractive index of the film stabilised.

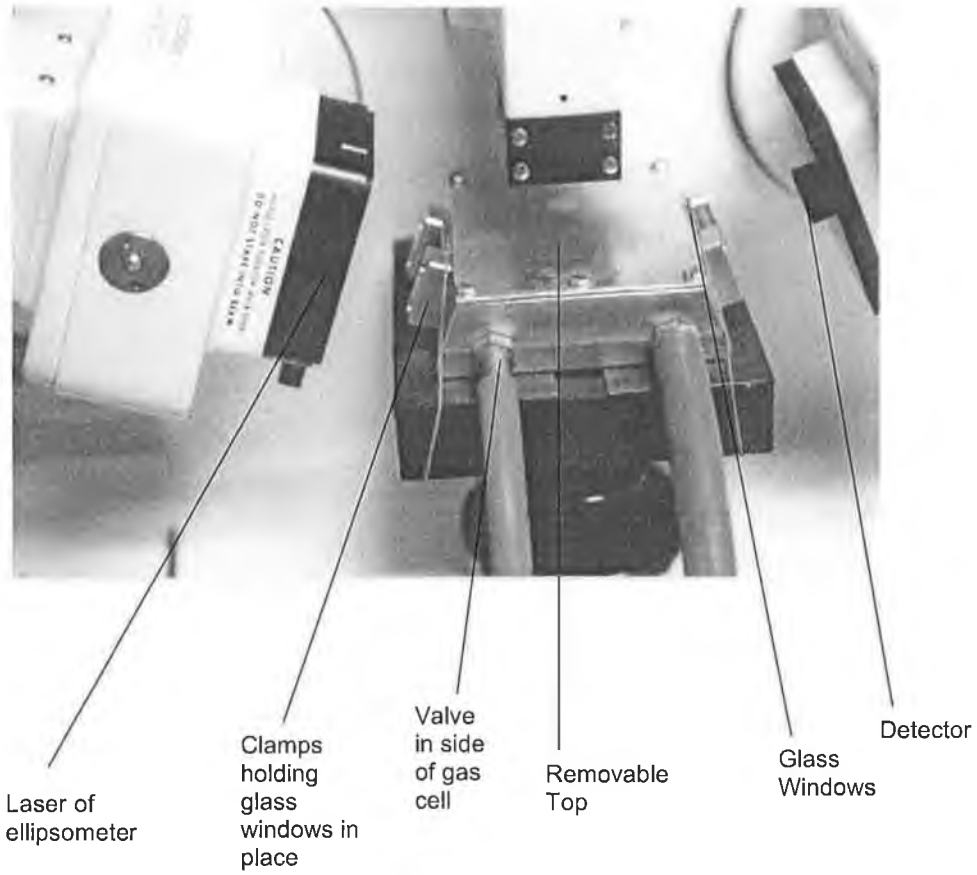


**Figure 4.3:** Experimental set-up used to calculate the porosity of sol-gel samples, showing the gas cell placed on the sample table of the ellipsometer.

By means of the Lorentz-Lorenz relationship [11] shown below, the porosity $V_p$, can be calculated:

$$\left(\frac{n_f^2-1}{n_f^2+2}\right) = (1-V_p)\left(\frac{n_s^2-1}{n_s^2+2}\right) \tag{4.1}$$

where $n_f$ is the stabilised refractive index of the film after dry $N_2$ is flowed over the surface of the film, $n_s$ is the refractive index of densified silica and has a value of 1.460 for TEOS and 1.453 for MTEOS at $\lambda$=633nm.

This technique is only an approximation, as the Lorentz-Lorenz relation does not include the effect of anisotropy on refractive index, or quantum mechanical effects which may be present for structures of near-atomic dimensions. Also porosity measurements ere only carried out in undoped sol-gel samples. However, the consistency of results obtained indicates that the approximation is good.

## 4.8 Experimental procedure to measure response time of sol-gel thin films

### 4.8.1 Experimental procedure

The experimental equipment required to measure the response time consisted of a vacuum pump, solenoid valve (ASCO), a National Instruments (PCI-6024E) data acquisition card, a lock-in amplifier (*EG&G* Princeton Applied Research), a photodiode (Hamamatsu) and a blue LED. The sol-gel based oxygen sensitive film was incorporated inside the solenoid valve of very small volume of approximately 5 cubic centimeters and illuminated by the blue LED as seen in Figure 4.4.

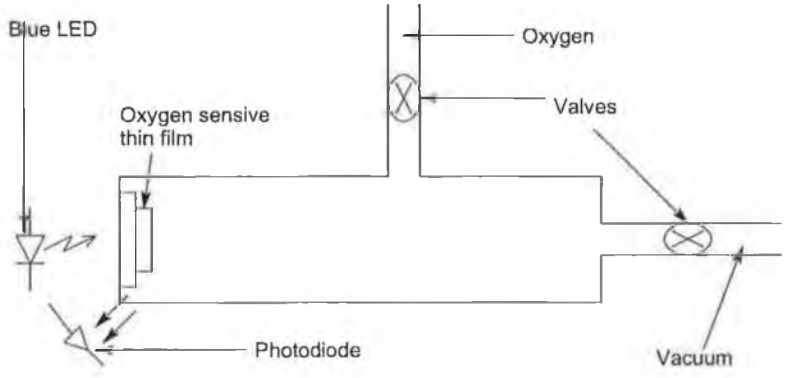


**Figure 4.4:** Schematic diagram of a oxygen sensitive sol-gel based thin film incorporated inside a solenoid valve

The emitted fluorescence after having passed through a optical filter (Lee 135) to

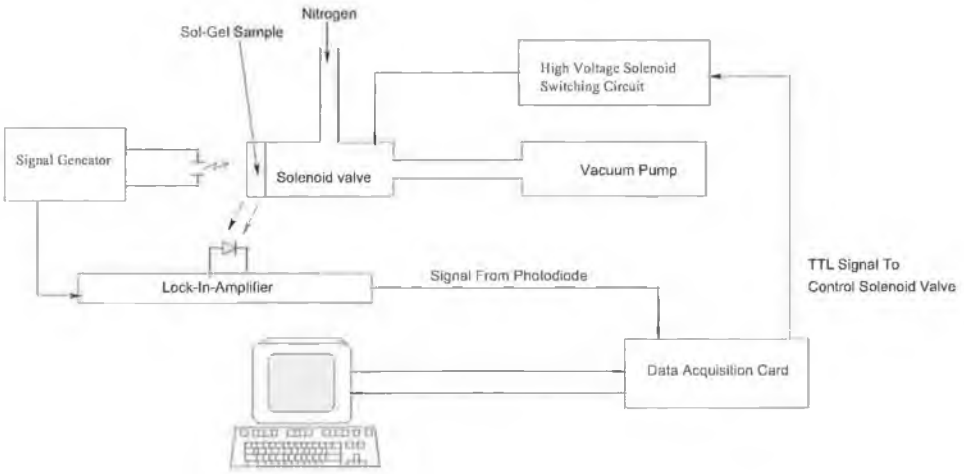


**Figure 4.5:** Diagram showing the experimental set-up used to measure the response times of sol-gel films.

block blue light from the photodetector was collected from the edge of the film [13] using a photodiode and was then fed into the lock-in amplifier. Edge detection is an efficient means of gathering light from the film. The LED modulation frequency was used as a reference for the lock-in amplifier. The output signal from the lock-in amplifier was then processed by the National Instruments data acquisition card under the control of a Labview program.

A gas handling system was used to switch the environment inside the solenoid valve from an oxygen to a vacuum environment. Hence the sol-gel oxygen sensitive film was exposed to alternative environments of oxygen and vacuum, resulting in the quenching and recovery of fluorescence emitted from the film. The switching of the solenoid valve was also controlled by the data acquisition card under the control of a Labview program. The data acquisition card generated a TTL signal that was fed to a high voltage solenoid switching circuit. This circuit ensured the fast switching of the valve. A schematic diagram showing the experimental set-up can be seen in Figure 4.5. The response time of the solenoid valve was quoted as approximately 5ms in its specifications sheet, while the National Instruments data acquisition card which was used to switch the valve open and closed has a voltage rise time of approximately 1$\mu$second. This makes the overall response time of the system approximately 5ms.

### 4.8.2 Labview

The signal from the photodiode was processed by a digital acquisition card. The card was controlled by a Labview programme written for this purpose. This section briefly describes the Labview language and the programs developed in this work.

Labview is a program development application such as other languages like C or Basic. However Labview is different from those applications in one respect. Other programming tools use text-based languages to create lines of code. Labview uses a graphical programming language, G, to create programs in block diagram form. Labview uses icons and graphical symbols to describe programming actions.

Labview has specific libraries of functions and subroutines for the majority of programming tasks. Specific libraries are available for the data acquisition card used in this experimental set-up.

Labview programs are called virtual instruments (VI's). VI's have 2 main parts: the front panel and the block diagram. The front panel is the interface the user sees and uses. It could display digital readings or wavecharts of how a signal is behaving in real-time in an experiment. The block diagram contains the Labview program. Figure 4.6 shows the front panel for the program used in this work. The block diagram or the Labview programme used to acquire the fluorescence from the sol-gel thin film is detailed in Appendix C.

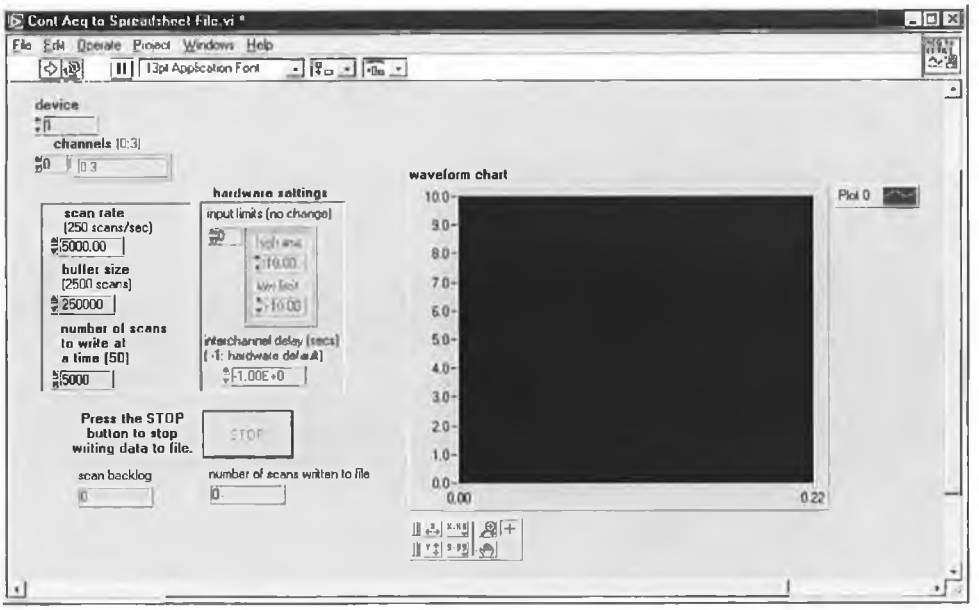


**Figure 4.6:** Shows the front-panel of the Labview wrote to record the signal from the photodiode

From Figure 4.6, it can be seen that a number of different options have to be updated before a reading can be made. The device option is usually not changed and is set when the data acquisition card has been installed for the first time on the computer. The channel number is the channel from which the signal from the photodiode is read. The scan rate is the number of scans read per second by the card. This was set to 5000 scans/s. Since so many readings are taken over a period of time, the Labview program, instead of writing all readings directly to a file, they are wrote to a buffer file first and then to the desired file, so as to achieve continuous acquisition. This is to prevent data being overwritten if the computer is unable to write to the file fast enough. The next option is the number of scans to write at a time. This specifies the number of scans to be written to a file from the buffer per second. The scan backlog showed whether or not there was a backlog in the buffer. If this figure was larger than the buffer size, then data would have been overwrote and lost. The number of scans written to file showed whether all expected scans were written to the specific file. The waveform chart showed a live image of how the signal was behaving. When the *'Go'* button was pressed (arrow in top left corner) a save dialog box appeared, allowing the user to save the data to a specific file. Using this program, the rapidly changing signal from the photodiode was recorded.

A Labview program was also written for the control of the solenoid valve as seen in Figure 4.7. Using this program, a TTL signal was sent from the data acquisition card to a high voltage solenoid switching circuit. The high voltage solenoid switching circuit was connected to the solenoid valve. This circuit ensured the fast switching of the solenoid valve. To switch the valve, the amplitude of the square wave was set to 6 volts. The update rate, recorded in seconds, specified how long the valve remained in a given position. Using this Labview program, the user could control the period of time the sensing film was exposed to a given atmosphere. The block diagram of the Labview program can be seen in Appendix D.

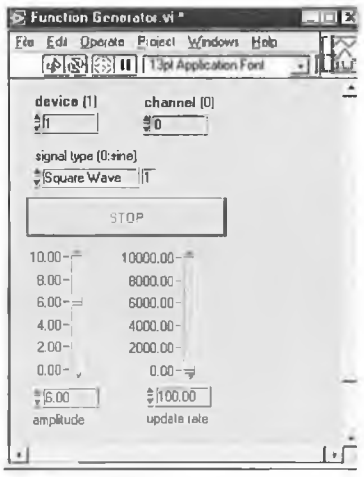


**Figure 4.7:** Front panel of Labview program used to create a TTL signal to control the opening and closing of the solenoid valve

## 4.9 Refractive index measurements

As well as using the ellipsometer to make refractive index and thickness measurements, a Metricon Model 2010 Prism Coupler was used. The principal components of the model 2010 include a photodetector, laser, prism and a coupling head as seen from Figure 4.8(a). A laser beam strikes the base of a high refractive index prism and is reflected onto a photodetector. The film to be measured is brought into contact with the prism base by means of a pneumatically-operated coupling head. The angle of incidence $\theta$, of the laser beam can be varied by means of a rotary table upon which the prism, film, coupling head and photodetector are mounted. At certain values of $\theta$, called mode angles, photons violate the total internal reflection criterion and tunnel from the base of the prism causing a sharp drop in intensity of light striking the photodetector [14]. This is due to a thin film of air trapped between the film and the pneumatically-operated head.

If the intensity striking the photodetector is plotted as a function of the angle $\theta$, a characteristic plot similar to Figure 4.8 (b) will be seen [14]. For a given substrate, the angular location of the modes depends only on film thickness and refractive index. Thus as soon as two modes are measured, the film thickness and refractive index can be measured using a computer algorithm. This method is a quick and extremely precise method of measuring thickness and refractive index.

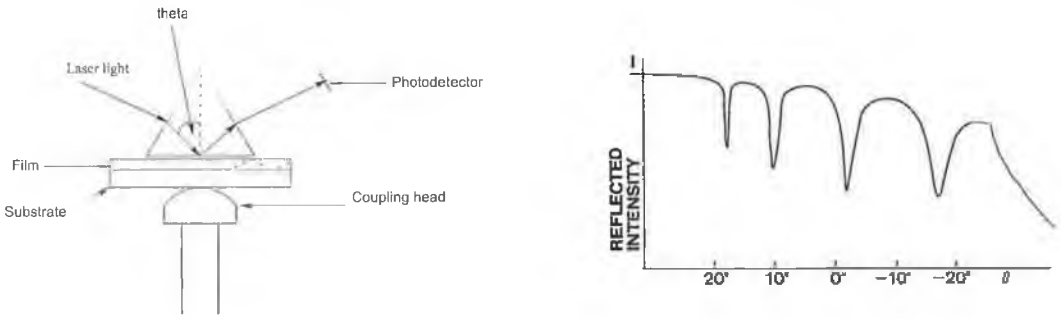


(a) (b)

**Figure 4.8:** (a) Shows the principal components of the Metricon and (b) the change in intensity of the light entering the photodetector with rotary angle, $\theta$

## 4.10 Thickness measurements

As mentioned in Section 4.7.2 the ellipsometer only returns a thickness value equal to: thickness+m(ordinate), where m is some integer. The Metricon is only able to measure the refractive index and thickness of films greater than approximately 1$\mu$m. As a result, another method had to be used to measure the thickness of films.

The Dektak V 200-Si was used for this purpose. This instrument is an advanced surface texture measuring system that accurately measures surface texture below 250$\mu$m [15]. Measurements are made electromechanically by moving the sample beneath a diamond-tipped stylus. The high precision stage moves a sample beneath the stylus according to a user programmable scan length, speed and stylus force. As the stage moves the sample, the stylus rides over the sample surface. Surface variations cause the stylus to be translated vertically. Electrical signals corresponding to the stylus movement are produced and mapped to produce a signal scan that can be displayed and analysed using Dektak's software.

## 4.11 Contact angle measurements

The contact angle, $\theta$, is a quantitative measure of the wetting of a solid by a liquid. It is defined geometrically as the angle, $\theta$, formed by a liquid at the three phase boundary where a liquid, gas and solid interact as seen in Figure 4.9.

The smaller the angle, the easier the liquid spreads over the surface of the solid and the more hydrophilic the surface, as seen in Figure 4.9(a). In contrast for large contact angles, the liquid does not wet the surface indicating a hydrophobic surface,

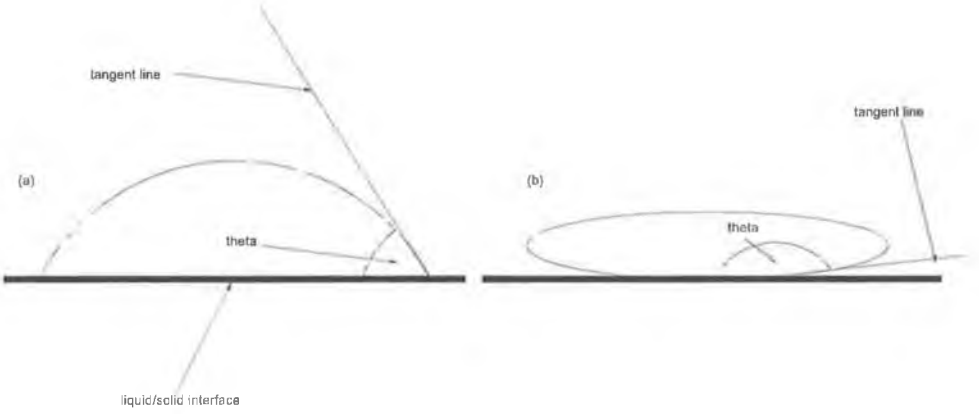


**Figure 4.9:** Contact angles for (a) hydrophilic and (b) hydrophobic solid surfaces

as seen in Figure 4.9(b).

Contact angle measurements were made on a Cahn Dynamic Contact Angle Analyser (DCA-315), which uses the tensiometric method to calculate a contact angle value. The tensiometric method measures the forces that are present when a sample of solid is brought into contact with a test liquid [16]. If the forces of interaction, geometry of the solid and surface tension of the liquid are known, the contact angle can be calculated. The user first has to make a measurement of the surface tension of the liquid using the user program on the computer. The sol-gel sample is then placed on the balance and tared. The sample is lowered to the liquid. When it strikes the liquid surface the change in the forces acting on the sample is detected and recorded. The forces on the sample are:

$$F_{TOTAL} = (wetting\ force) + (weight\ of\ the\ probe) - (buoyancy) \tag{4.2}$$

The computer algorithm calculates the total force acting on the sol-gel sample, as well as the weight and buoyancy. The remaining component is the wetting force, defined as: wetting force=$\gamma_{LV} PCos\theta$, where $\gamma_{LV}$ is the already calculated surface tension of the liquid, P is the wetted perimeter of the sol-gel slide and is equal to the width of the sol-gel slide and $\theta$ is the contact angle. The contact angle which is obtained from data generated as the probe advances into the liquid is called the advancing contact angle. The sample is immersed to a set depth and the process is reversed. As the probe retreats from the liquid the data collected is used to calculate a receding contact angle. When making contact angle measurements perspex slides

were prepared and dip-coated with the sol under investigation, resulting in a sol-gel film forming on both faces of the perspex slide. This was done to ensure that both sides of the slide have the same contact-angle properties.

## 4.12 Conclusion

This chapter detailed the methods used to fabricate a wide range of sol-gel-derived material, including TEOS, MTEOS and phenyl based films. By careful manipulation of the tailoring techniques it was possible to control various attributes of the sol-gel such as porosity and thickness.

An experimental system was developed, in order to measure the porosity of sol-based films. It consisted of a sample placed in a specially designed gas cell, which in turn was placed on the sample table of an ellipsometer. The resulting porosity was measured using both the Lorentz-Lorenz equation and the values of refractive index returned by the ellipsometer.

A system used to measure the response time of a gas sensor was developed. The gas exchange time of the measurement chamber was minimised as this exchange time normally masks the underlying intrinsic sensor response time. Response time measurement was achieved by incorporating a miniature oxygen sensor in a fast solenoid valve. The oxygen-dependent fluorescence was detected from the film and processed using a Labview program.

The range of different instrumentation used to characterise the sol-gel films was also detailed. This included contact analyser, refractive index measurement system and a profilmeter.

# Bibliography


[1] M.A. Farad, E.M. Yeatman, E.J.C. Dawnay, Mino Green, and F. Horowitz. Effects of h2o on structure of acid-catalysed sio2 sol-gel films. *Journal of Non-crystalline Solids*, 183:260–267, 1995.

[2] E.M.Yeatman, Mino Green, E.J.C. Dawnay, M.A. Fardad, and F. Horowitz. Characterisation of microporous sol-gel films for optical applications. *Journal of Sol-Gel Science and Technology*, 2:711–715, 1994.

[3] Alan E. Baron, J.D.S. Danielson, Martin Gouterman, Jiang River Wan, James B. Callis, and Blair McLachen. Submillisecond response times of oxygen quenched luminescent coatings. *Review of Scientific Instruments*, 64(12):3394–3402, 1993.

[4] R.J. Watts and G.A. Crosby. *Journal of American Chemical Society*, (93):3184, 1971.

[5] Aisling McEvoy. *Development of an optical sol-gel based dissolved oxygen sensor.* PhD thesis, Dublin City University, 1996.

[6] G.R. Aitkins, R.M. Krolikowska, and A. Samoc. Optical propteries of an ormosil system comprising methyl- and phenyl-substituted silica. *Journal of Non-Crystalline*, 265:210–220.

[7] I. Klimant, F. Ruckruh, G. Liebsch, A. Stangelmayer, and O.S. Wolfbeis. Fast response oxygen micro-opodes based on novel soluble ormosil glasses. *Mikrochimica Acta*, 131:35–36, 1999.

[8] P Lavin, C.M. McDonagh, and B.D. MacCraith. Optimization of ormosil for optical sensor applications. *Journal of Sol-Gel Science and Technology*, 13:641–645, 1998.

[9] C.J. Brinker, A.J. Hurd, P.R. Schunk, G.C. Frye, and C.S. Ashley. Review of sol-gel thin film formation. *Journal of Non-Crystalline Solids*, 147,148:424–436, 1992.

[10] Karl Riedling. *Ellipsometry for industrial applications.* Springer-Verlag Wien, New York, 1988.

[11] M. Born and E. Wolf. *Principles in Optics.* Academic Press, London, 1980.

[12] Rui M. Almeida. Sol-gel silica films on silicon substrates. *International Journal of Optoelectronics*, 9(2):135–142, 1994.

[13] J.F. Gouin, A. Doyle, and B.D. MacCraith. Fluorescence capture by planar waveguides as platform for optical sensors. *Electronic Letters*, 34:1685–1687, 1998.

[14] Metricon model 2010 prism coupler thin film thickness/refractive index measurement system operating guide and maintenance guide, 1991.

[15] Installation operation and maintenance cleanroom manual for dektak v 200-si 200mm wafer surface profiler.

[16] http:/www.ksvinc.com.

# Chapter 5

# Porosity measurements of sol-gel films

## 5.1 Introduction

The use of sol-gel technology to produce various sensors has been widely studied by this research group [1, 2, 3, 4, 5, 6, 7]. Oxygen sensors have received most attention and in the majority of cases the sol-gel matrix acts as a support for the oxygen sensitive luminescent metal complex, $[Ru(Ph_2phen)_3]Cl_2$ ($Ph_2phen = 4,7-diphenyl-1,10-phenanthroline$). The analyte molecules, in this case, oxygen, may therefore diffuse through the matrix and interact with the ruthenium complex resulting in the quenching of fluorescence [2].

The porosity of the sol-gel matrix plays a vital role in the sensitivity and response time of sol-gel based optical oxygen sensors. Satoh et al. [8] reported an increase in the diffusion coefficient with porosity. This has the effect of increasing the sensitivity of the sensor via the Stern-Volmer equation as described in Section 3.4. The response and recovery times of the sensor are also related to porosity via the gas diffusion coefficient [9].

Using the experimental apparatus described in Chapter 4 porosity was measured for a range of sol-gel derived films and correlated with predicted film behavior and also with previous characteristic studies.

## 5.2 Results and discussion

### 5.2.1 Porosity of TEOS samples

#### 5.2.1.1 Influence of aging time and R-value

The porosity of TEOS films was investigated as a function of aging time and R-value. As already mentioned, aging is the time between mixing the sol and dip-coating and usually occurs at elevated temperatures (Section 2.2.3). During this period of time, hydrolysis and condensation occur leading to more crosslinking and increased porosity [10]. The results of this investigation are shown in Figure 5.1. It can be seen that porosity decreases with increasing R-values (R=2 to R=4) for a given aging time, while, for a given R-value, porosity increases with increasing aging time.

The increase in porosity with increasing aging time and decreasing R-value is expected. As hydrolysis and condensation proceed, they give rise to increased crosslinking and growth of particles in the sol, resulting in an increase in porosity [11]. This point was described previously in Section 2.3.1.

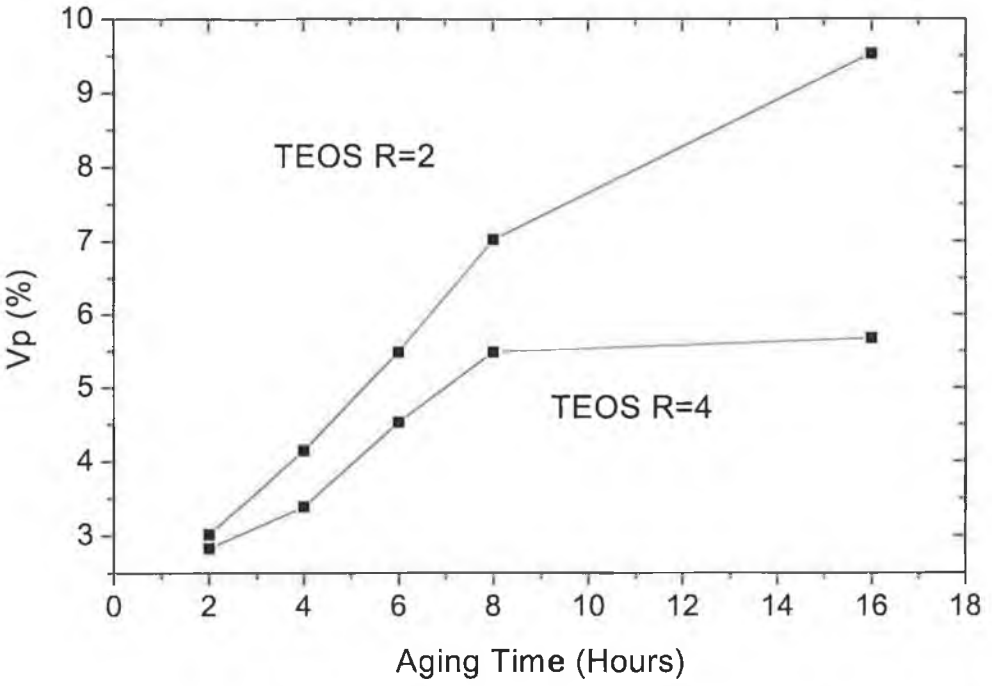


**Figure 5.1:** Dependence of porosity, $V_p$, on aging time and R-value for TEOS R=2 and R=4 films

#### 5.2.1.2 Influence of ethanol:TEOS ratio

The porosity values of TEOS R=4 samples were measured when the ethanol:TEOS ratio was varied using the discrete values: 1.5, 2 and 3. From Section 2.3.3 it was seen that increasing the amount of ethanol has the effect of slowing down the gelation and hydrolysis process.

As seen in Figure 5.2, the porosity, ($V_p$), decreased with increasing ethanol:TEOS ratio. This behavior is consistent with the retardation of the gelation process with higher ethanol content, resulting in slower particle growth processes and reduced crosslinking in the sol and a consequent reduction in porosity [12].

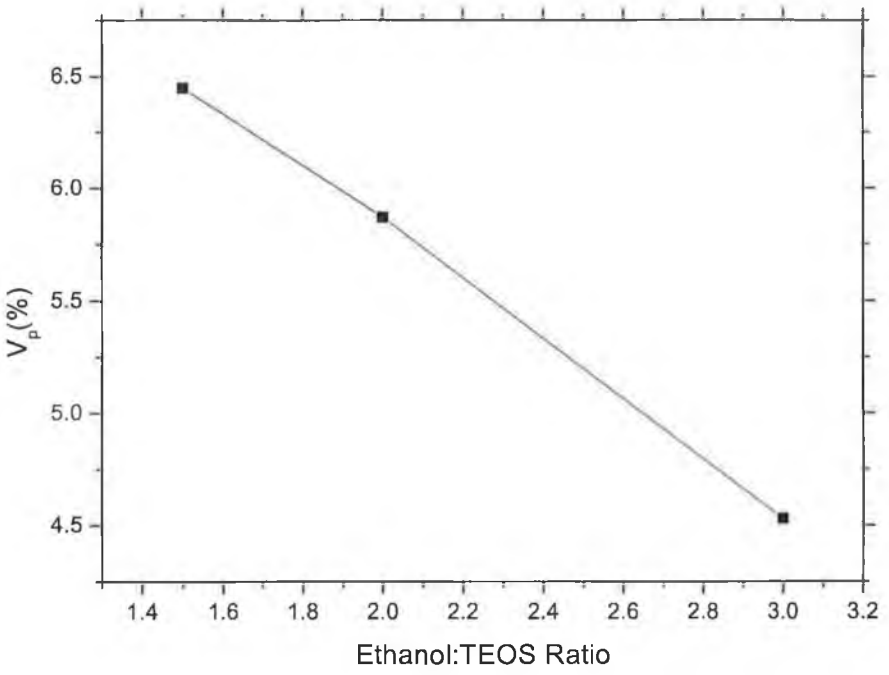


**Figure 5.2:** Dependence of porosity, $V_p$, when EtOH:TEOS ratio is increased for TEOS R=4

#### 5.2.1.3 Influence of sol pH

Sol pH plays a vital role in the determination of the film microstructure. Table 5.1 compares the porosity of TEOS films fabricated at two different pH values, 1 and 4. For both aging times the porosity is higher at higher pH. Films fabricated at pH1 are derived from weakly branched systems where hydrolysis rates are very fast and condensation is inhibited. At low aging times, this gives rise to interpenetrating

dense microporous structures with low porosity. It is clear that, even for these weakly branched structures, aging enhances the porosity.

Under more basic conditions (pH4 films), hydrolysis is slower and the condensation rate is faster. The film microstructure evolves by growth of particles within the sol producing more porous films with higher average pore size. From Table 5.1, it is clear that, for a given aging time, porosities increase considerably between the two pH regimes which is consistent with predicted behavior.

| Aging Time (hours) | Porosity ($V_p$) at pH1 (%) | Porosity ($V_p$)at pH4 (%) |
|---|---|---|
| 4 | 3.4 | 4.5 |
| 6 | 4.5 | 8.0 |

**Table 5.1:** Dependence of porosity, $V_p$, using the catalyst HCl at pH1 and 4, for TEOS R=4 films aged for 4 and 6 hours

### 5.2.2 Porosity of MTEOS samples

The porosity of R=2 and R=4 MTEOS films was measured and the results are shown in Table 5.2.

| R-value | $V_p$ (%) |
|---|---|
| 2 | 5.2 |
| 4 | 2.6 |

**Table 5.2:** Porosity, $V_p$, of MTEOS samples with the R-value varied

From Table 5.2 it can be seen that porosity decreases when the R-value goes from R=2 to R=4. As already mentioned, the increase in R-value promotes hydrolysis producing a more highly branched system with a lower porosity.

When using Equation 4.1 to calculate the porosity of MTEOS, the value used for the skeleton refractive index, $n_s$, is 1.453, This value was calculated after the refractive index of densified MTEOS was measured. The MTEOS film was densified at approximately 700°C for 45 minutes. This lower value of $n_s$ for MTEOS compared to TEOS is as expected, as the introduction of methyl substitutes reduces the refractive index of silica [13].

### 5.2.3 Comparison of porosities of TEOS and MTEOS films

For both film types, $V_p$ decreases with increasing R-value. This trend is consistent with an increased hydrolysis rate due to higher water content in the sol, resulting in a denser microstructure and smaller average pore radius. When comparing TEOS and MTEOS films, the overall porosity of TEOS films is higher than MTEOS, particularly at the longest aging times for TEOS films. This is consistent with the literature prediction [14, 15] of higher reaction rates for organically modified precursors resulting in dense microstructural films and hence lower porosity compared to TEOS films.

## 5.3 Difficulties encountered in making porosity measurements

Originally an alternative method to measure porosity was used. This method was based on the use of humidified gas and follows the work of Farad et al. [11], whereby the refractive index of microporous films depends strongly on relative humidity, because condensation occurs in the pores. By measuring this dependence, information on the porosity of a microporous sample can be obtained. In this technique, similar to the method described in Section 4.7, the sample is placed in a gas cell which is placed on the sample table of an ellipsometer. Dry $N_2$ gas is flowed through the gas cell until the decreasing refractive index stabilises. Water saturated $N_2$ (having been bubbled through water) is then passed through the gas cell and over the sample. The refractive index is seen to increase and stabilise. The assumption is made that all accessible pores in dry and wet atmospheres are empty and full, respectively. Using this method the porosity, $V_p$, and the skeleton index, $n_s$, is obtained using the modified Lorentz-Lorenz equation:

$$\left(\frac{n_f^2-1}{n_f^2+2}\right) = (1-V_p)\left(\frac{n_s^2-1}{n_s^2+2}\right) + V_p\left(\frac{n_p^2-1}{n_p^2+2}\right) \tag{5.1}$$

where $n_f, n_s$ and $n_p$ are the refractive indices of the film, solid skeleton and pores respectively. By measuring $n_f$, the stabilised refractive index, for both dry and saturated conditions, both $V_p$ and $n_s$ can be calculated from the resulting pair of simultaneous equations ($n_p$ is chosen to be 1 in the case of dry $N_2$, and 1.333 in the case of water-saturated $N_2$).

Using this method, the values calculated for $n_s$ were not as expected. In some instances values greater than 1.46 and in others values less than 1.42 were calculated. This is not possible as densified TEOS has a refractive index of 1.46. The samples under investigation here are not densified and therefore should not have a refractive index greater than 1.46. The same problems were also associated with MTEOS films.

Since this method proved unsatisfactory in the calculation of porosity the simplified version of the Lorentz-Lorenz equation was used (Equation 4.1).

## 5.4 Conclusion

The porosity results indicate the ease at which the sol-gel matrix can be tailored and modified. An increase in porosity was seen for both R=2 and R=4 films when the aging time was increased from 2 to 16 hours, R=2 films having the largest porosity.

The ethanol:TEOS ratio was varied using the values: 1.5, 2 and 3, resulting in a decrease in porosity for an increase in ethanol content.

The impact of the pH of the catalyst on the microstructure of the sol-gel film was observed. A high pH gives a greater porosity although film quality is compromised. MTEOS films proved, as expected, to have a more dense microstructure with a lower porosity.

A number of difficulties were encountered in the development of a method to calculate porosity. These were overcome to give a method capable of predicting correct trends in porosity according to the tailoring techniques used to fabricate the films.

It was noted that TEOS R=2 and R=4 films fabricated using a catalyst at pH1 and with an ethanol:TEOS ratio of 3 produced the best quality films. Within this, film quality increased with aging time up to a limit where increased periods of aging led to cracking of the film.

# Bibliography


[1] A.K. McEvoy, C. McDonagh, and B.D. MacCraith. Optimisation of sol-gel derived silica films for optical oxygen sensing. *Journal of Sol-Gel Science and Technology*, 8:1121–1125, 1997.

[2] B.D. MacCraith, C.M. McDonagh, G. O'Keefe, A.K. McEvoy, T. Butler, and F.R. Sheridan. Sol-gel coatings for optical chemical sensors and biosensors. *Sensors and Actuators B*, 29:51–57, 1995.

[3] G O'Keeffe, B.D. MacCraith, A.K. McEvoy, C.M. Mc Donagh, and J.F. McGlip. Development of a led-based phase fluorimetric oxygen sensor using evanescent wave excitation of a sol-gel immobilized dye. *Sensors and Actuators B.*, 29:226–230, 1995.

[4] B.D. MacCraith, C. McDonagh, A. K. McEvoy, T. Butler, G. O'Keeffe, and V. Murphy. Optical chemical sensors based on sol-gel materials: Recent advances and critical issues. *Journal of Sol-Gel Science and Technology*, 8:1053–1061, 1997.

[5] C. McDonagh, C.Kolle, A.K. McEvoy, D.L. Dowling, A.A. Cafolla, S.J. Cullen, and B.D. MacCraith. Phase fluorometric dissolved oxygen sensor. *Sensors and Actuators B: Chemical*, 74:124–130, 2001.

[6] C. McDonagh, B.D. MacCraith, and A.K. McEvoy. Tailoring of sol-gel films for optical sensing of oxygen in gas and aqueous phase. *Analytical Chemistry*, 70:45–50, 1998.

[7] P Lavin, C.M. McDonagh, and B.D. MacCraith. Optimization of ormosil for optical sensor applications. *Journal of Sol-Gel Science and Technology*, 13:641–645, 1998.

[8] S. Satoh, I. Matsuyama, and K. Susa. Diffusion of gases in porous silica gel. *Journal of Non-Crystalline Solids*, 190:206–211, 1995.

[9] A. Mills and Q. Chang. Modelled diffusion-controlled response and recovery behaviour of a naked optical film sensor with a hyperbolic response to analyte concentration. *Analyst*, 117:1461–1466, 1992.

[10] C. Jeffrey Brinker and George W. Scherer. *Sol-Gel Science: The Physics and Chemistry of Sol-Gel Processing.* Academic Press Inc., San Diego, 1990.

[11] M.A. Farad, E.M. Yeatman, E.J.C. Dawnay, Mino Green, and F. Horowitz. Effects of H2O on structure of acid-catalysed SiO2 sol-gel films. *Journal of Non-Crystalline Solids*, 183:260–267, 1995.

[12] Sasa Wang, Honhliu Liu, Liangying Zang, and Xi Yao. Pore size control of porous silica by sol-gel process. *Feroelectric Letters*, 19:89–94, 1995.

[13] Graham R. Atkins, R. Maryla Kroilikowska, and Anna Samoc. Optical properties of an ormosil system comprising methyl- and phenyl-substituted silica. *Journal of Non-Crystalline Solids*, 265:210–220, 2000.

[14] H. Schmidt, H. Scholse, and A. Kaiser. *Journal of Non-Crystalline Solids*, 63:1, 1984.

[15] P. Innocenzi, M.O. Abdirashid, and M. Guglielmi. Structure and properties of sol-gel coatings from methyltriethoxysilane and tetraethoxysilane. *Journal of Sol-Gel Science and Technology*, 3:47–55, 1994.

# Chapter 6

# Response times and diffusion coefficients of sol-gel thin films

## 6.1 Introduction

This chapter focuses on using the porosity results detailed in Chapter 5 and measured sensor response times, detailed in this chapter, to characterise the oxygen sensing behavior of a wide range of TEOS and MTEOS films. Measured response times were correlated with porosity data and oxygen sensor quenching data. Diffusion coefficients were estimated by modelling the sensor response. The unquenched lifetime of the fluorophore was measured for a range of films. These lifetime data, together with diffusion coefficient data and Stern-Volmer constants, were used to investigate gas solubility behavior in the films.

## 6.2 Measurement of response times and diffusion coefficients

The oxygen sensor response times, $t_{90}$, for both TEOS and MTEOS films, were measured using the technique described in Section 4.8. The oxygen diffusion coefficient, D, a more fundamental parameter than the response time was also calculated. D was calculated using the technique described in Section 3.5.

Typical examples of the behavior of the intensity of the fluorescence from a sol-gel sample with time can be seen in Figures 6.1 and 6.2, showing the asymmetrical response-recovery behavior of optical sensors with a hyperbolic response. Figures

6.1 and 6.2 also show how the recovery, ($t_{90}(\uparrow)$), and response, ($t_{90}(\downarrow)$), times of a sample are obtained.

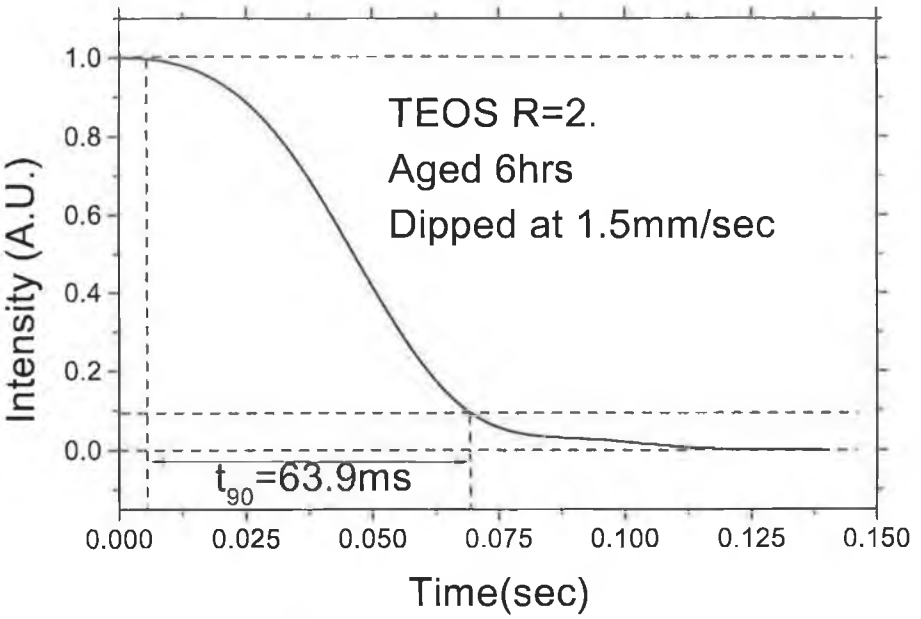


**Figure 6.1:** Change in intensity of fluorescence of a sol-gel sample when going from vacuum to $O_2$. The response time, $t_{90}(\downarrow)$, is calculated as shown

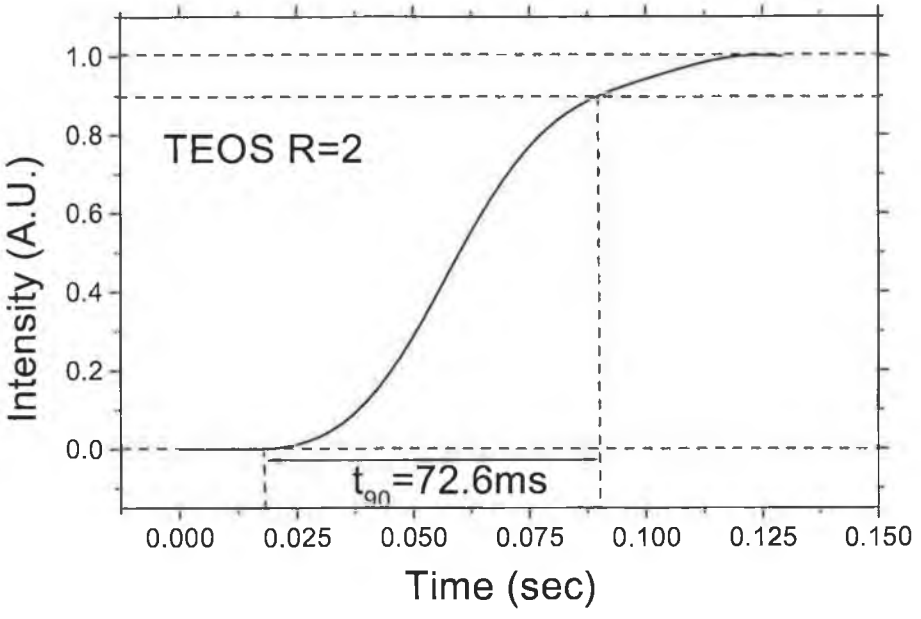


**Figure 6.2:** Change in intensity of fluorescence of a sol-gel sample when going $O_2$ to vacuum. The recovery time, $t_{90}(\uparrow)$, is calculated as shown

Response times, porosities and the corresponding diffusion coefficients for a range of films are given in Tables 6.1, 6.2 and 6.3.

| Sample | Aging time (hours) | D ($cm^2s^{-1}$) | $V_p$ (%) | $t_{90}$(ms) |
|---|---|---|---|---|
| TEOS R=2 | 4 | $5.0 \times 10^{-9}$ | 4.2 | 106.2 |
| | 6 | $1.5 \times 10^{-8}$ | 5.5 | 77.8 |
| | 16 | $3.2 \times 10^{-8}$ | 9.5 | 40.2 |
| TEOS R=4 | 6 | $3.5 \times 10^{-9}$ | 4.5 | 538.8 |
| | 16 | $8.8 \times 10^{-9}$ | 5.7 | 462.2 |

**Table 6.1:** Calculated diffusion coefficients, porosities and response times for a range of TEOS films.

| Sample | D ($cm^2s^{-1}$) | $V_p$ (%) | $t_{90}$(ms) |
|---|---|---|---|
| TEOS R=2 | $2.3 \times 10^{-8}$ | 6.5 | 67.7 |
| TEOS R=4 | $1.1 \times 10^{-8}$ | 5.9 | 148.9 |

**Table 6.2:** Calculated diffusion coefficients, porosities and response times for TEOS R=2 and 4 films with an ethanol:TEOS ratio of 2 and aged for 6hrs

| Sample | D ($cm^2s^{-1}$) | $V_p$ (%) | $t_{90}$(ms) |
|---|---|---|---|
| MTEOS R=2 | $7.8 \times 10^{-8}$ | 5.2 | 10.2 |
| MTEOS R=4 | $5.9 \times 10^{-8}$ | 2.6 | 19.2 |

**Table 6.3:** Calculated diffusion coefficients, porosities and response times for a MTEOS R=2 and 4

As expected, for TEOS films, (Tables 6.1 and 6.2 ), both response times and diffusion coefficients are directly correlated with porosity.

From Table 6.3, it is clear that MTEOS films exhibit response times that are considerably smaller, for films with similar thickness, when compared to TEOS films. The MTEOS diffusion coefficients are correspondingly larger. The absolute values of porosity for MTEOS films were shown to be smaller than for TEOS films due to faster hydrolysis and condensation reactions [1, 2]. Hence the higher diffusion coefficient could not be as a result of greater porosity. It is therefore thought that

the diffusion of oxygen in MTEOS and TEOS films is due to a complex process related to the hydrophobic/hydrophilic nature of the film. The nature of the surface of the film is discussed in the next section.

### 6.2.1 Hydrophobic/hydrophilic nature of sol-gel films

The reactions for hydrolysis and condensation were discussed in Section 2.2.2. When TEOS is hydrolysed, Si-OH bonds are formed. If these groups do not undergo condensation reactions they are termed terminal silanol groups. On the surface of a film fabricated using TEOS as a precursor, there are many of these silanol groups. These make the TEOS film very hydrophilic since water can become hydrogen-bonded to the SiOH surface. Figure 6.3 illustrates this point.

As a consequence, it is suggested that the diffusion process is more complex in TEOS due to the high concentration of water adsorbed on the hydrophilic surface. This diffusion process may involve oxygen continuously partitioning into and out of the water layer as the molecules move through the film, thereby giving rise to longer sensor response times and lower diffusion coefficients.

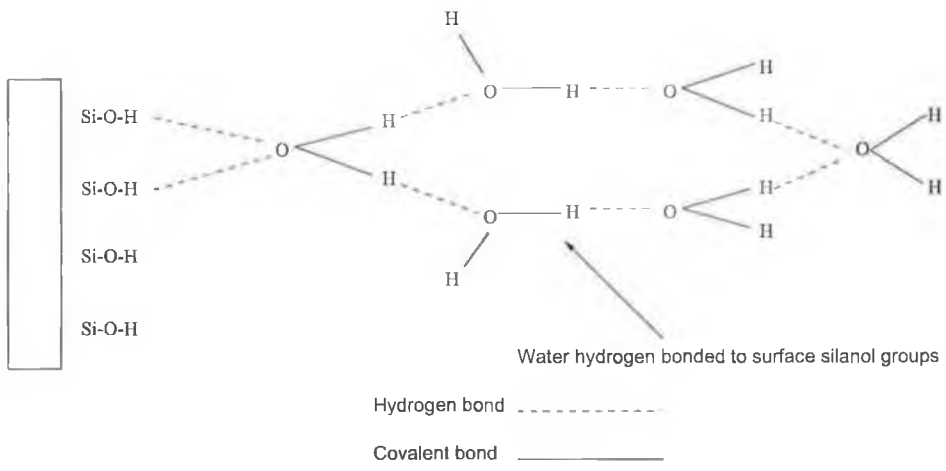


**Figure 6.3:** Water bonded to the surface of a TEOS film

On the other hand, MTEOS films are a typical example of films fabricated using a modified silicon alkoxide precursor, where a methyl group replaces one of the ethoxy groups. This methyl group is bonded to the silicon atom through a non-hydrolysable covalent bond and has the effect of making the film surface hydrophobic. The MTEOS film surface repels the water from the pore structure resulting in the easier passage of oxygen through the pore structure to interact with the ruthenium dye.

It can be seen therefore that the hydrophobicity of a sol-gel film is a crucial parameter. One method of measuring the hydrophobicity of a film surface is to use a contact angle measurement.

As discussed in Section 4.11, the smaller the angle, the easier the liquid spreads over the surface of the solid and the more hydrophilic the surface. In contrast for large contact angles, the liquid does not wet the surface, indicating a hydrophobic surface.

From Table 6.4 it can be seen that the contact angle for MTEOS is higher than that for TEOS. With an advancing angle of 85.4°, MTEOS is hydrophobic compared to the hydrophilic TEOS. The fact that MTEOS is hydrophobic compared to hydrophilic TEOS plays a vital role in the behavior and characteristics of sol-gel films when used as optical oxygen sensors. This will be discussed in the next section.

| Sample | Contact Angle (Advancing Angle) | Standard Deviation |
|---|---|---|
| MTEOS R=4 | 85.4° | 5.8° |
| TEOS R=4 | 39.2° | 5.0° |

**Table 6.4:** Contact angle measurements for MTEOS and TEOS samples

### 6.2.2 Consequence of hydrophobic nature of MTEOS films

As seen in the previous Section, MTEOS films are hydrophobic. This leads to the conclusion that little or no water forms on the film surface and as a result the pore structure is free from any obstructions. The oxygen molecules therefore have easy access via the pore structure to interact with the ruthenium metal complex in order to quench its fluorescence.

On the other hand, TEOS films are hydrophilic, meaning a water layer is formed on the surface of the film. Water molecules are adsorbed onto the pore walls and form a layer which effectively reduces the pore size [3]. This leads to the continuous partitioning into and out of the water layer of oxygen molecules as they move through the TEOS sol-gel film leading to long sensor response times and low diffusion coefficients compared to MTEOS films.

## 6.3 Correlation of Stern-Volmer constants with diffusion coefficients

In this section, the higher diffusion coefficient for MTEOS films compared to TEOS films is interpreted in terms of the oxygen quenching behavior.

As discussed in Section 3.4, the Stern Volmer coefficient, $K_{SV}$, is given by the slope of the Stern-Volmer equation. Referring to Equations 6.1 and 6.2, the Stern-Volmer coefficient for oxygen quenching, which is a measure of the oxygen sensitivity, is proportional both to the decay time, $\tau_0$, and the diffusion coefficient, D.

$$K_{SV} = k\tau_0 \tag{6.1}$$

and

$$K_{SV} = 3.4 \times 10^{12} SD\tau_0 \tag{6.2}$$

From Equations 6.1 and 6.2, it can be seen that the parameters which influence the sensitivity include the decay time, $\tau_0$, as well as the diffusion coefficient, D, and film solubility, S. It is clear from Table 6.5 and 6.6 that there is a clear correlation between Stern-Volmer coefficients and oxygen diffusion coefficients, as expected. For example, for TEOS films, the increase in $K_{SV}$ with aging time correlates with an increase in porosity and with a corresponding increase in D for these films. The film with the highest porosity (>9%) is TEOS aged for 16 hours which also is the largest $K_{SV}$ or oxygen sensitivity and consequently the largest diffusion coefficients for TEOS films.

| Sample | Aging time (hours) | $K_{SV}$ $(Torr^{-1})$ | D $(cm^2 s^{-1})$ | $V_p$ (%) |
|---|---|---|---|---|
| TEOS R=2 | 4 | .001852 | $5.0 \times 10^{-9}$ | 4.2 |
| | 6 | .005305 | $1.5 \times 10^{-8}$ | 5.5 |
| | 16 | .008519 | $3.2 \times 10^{-8}$ | 9.5 |
| TEOS R=4 | 6 | .004605 | $3.5 \times 10^{-9}$ | 4.5 |
| | 16 | .006608 | $8.8 \times 10^{-9}$ | 5.7 |

**Table 6.5:** Correlation between Stern-Volmer coefficient, $K_{SV}$, and diffusion coefficient, D, for TEOS R=2 and 4

As can be seen from Tables 6.5 and 6.6, there is a clear distinction between TEOS and MTEOS films with regard to diffusion coefficient. It can be seen that

| Sample | $K_{SV}$ $(Torr^{-1})$ | D $(cm^2s^{-1})$ | $V_p$ (%) |
|---|---|---|---|
| MTEOS R=2 | .004267 | $7.8 \times 10^{-8}$ | 5.2 |
| MTEOS R=4 | .003427 | $5.9 \times 10^{-8}$ | 2.6 |

**Table 6.6:** Correlation between Stern-Volmer coefficient, $K_{SV}$, and diffusion coefficient, D, for MTEOS films

while $K_{SV}$ for both TEOS and MTEOS films are similar, the $t_{90}$ response times are considerably smaller for MTEOS films, resulting in larger values of diffusion coefficient. For example, comparing TEOS R=4 aged for 6 hours with MTEOS R=2, the $K_{SV}$ values are comparable but the MTEOS film has a diffusion coefficient which is a factor of 20 larger.

Referring to Equations 6.1 and 6.2, the larger MTEOS diffusion coefficient must correspond to a smaller value of the product of decay time and solubility for MTEOS films compared to TEOS.

To investigate this further the unquenched lifetime in the absence of oxygen, $\tau_0$, for a range of sol-gel samples was measured. This will be discussed in the next section.

### 6.3.1 Unquenched lifetimes of the ruthenium complex

Unquenched lifetime measurements were made using a Q-switched Nd:YAG laser system (Quanta-Ray GCR2, with pulse width 9ns and emission wavelength of 365nm.) The resultant decay curves were fitted using the double exponential expression, $y = y_0 + A_1 e^{\frac{-x}{t_1}} + A_2 e^{\frac{-x}{t_2}}$. A double exponential expression was used to fit the lifetime decay curves because sites within the film matrix with different lifetimes and degrees of quenching contribute to the decay, therefore requiring a double exponential curve fit [4]. Figure 6.4 is an example of a double exponential curve fit.

| Sample | Aging time (hours) | $\tau_0$ ($\mu$s) |
|---|---|---|
| TEOS R=2 | 4 | 5.2 |
| | 6 | 5.1 |
| | 16 | 4.9 |
| TEOS R=4 | 6 | 5.1 |
| | 16 | 4.9 |

(a)

| Sample | $\tau_0$ ($\mu$s) |
|---|---|
| MTEOS R=2 | 4.9 |
| MTEOS R=4 | 4.9 |

(b)

**Table 6.7:** Unquenched lifetimes, $\tau_0$, of various (a) TEOS and (b) MTEOS films

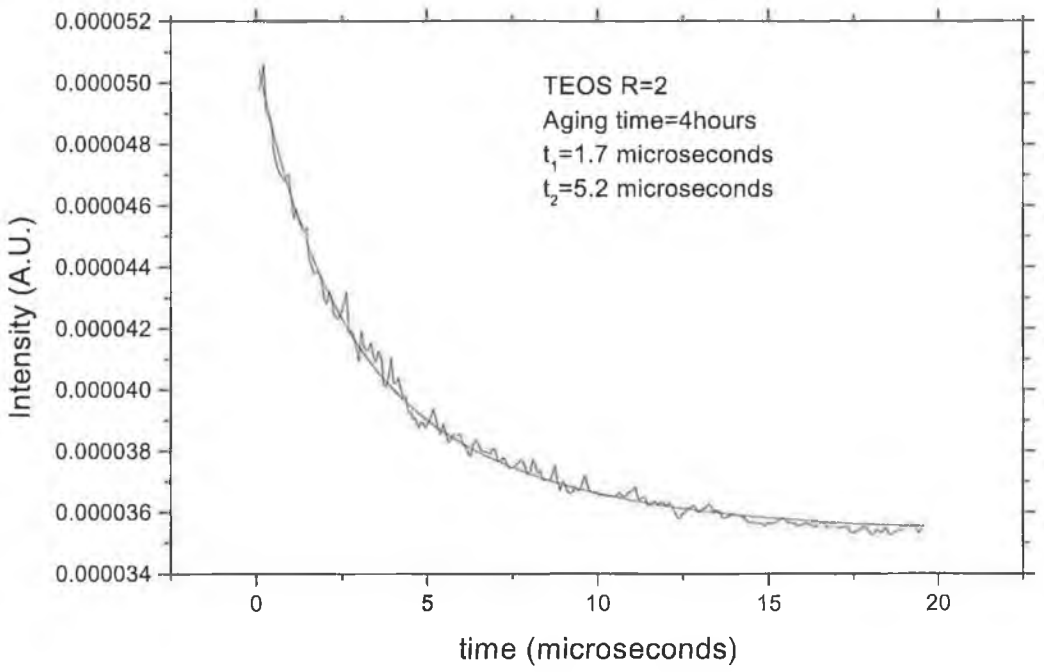


**Figure 6.4:** Decay curved fitted using a double exponential decay curve

It is clear from Table 6.7 that there is little variation in decay time for both TEOS films fabricated under different conditions and also between TEOS and MTEOS matrices. This is consistent with previous work where it was established that the ruthenium complex is relatively insensitive to the sol-gel matrix due to the presence of large phenyl rings outside the phenanthroline center [5, 6]. A change in the unquenched lifetime of the ruthenium complex is therefore not responsible for the large difference seen in diffusion coefficient values for TEOS and MTEOS samples. This would suggest that the oxygen solubility in the MTEOS matrix is considerably less (by a factor of $\sim$ 20) than in TEOS.

### 6.3.2 Oxygen solubility, S, of sol-gel films

The solubility of oxygen in a matrix as discussed in Section 3.4 obeys Henry's Law at low pressures. The mass of the gas dissolved is related to the free volume in the sol-gel matrix [7]. The polarisability of the matrix also has a minor effect. Recent studies on hydrophobic polymer films highlight the very small variation in oxygen solubility across a range of films [6]. For films such as silicone rubber, polystyrene and PMMA, the solubility parameter was measured to be in the order of 1 $\times 10^{-6} \mathrm{Pa}^{-1}$. Where

these films were used in oxygen sensor applications, however, the oxygen diffusion coefficients varied widely. Although the MTEOS ormosil films have some polymer characteristics, generally sol-gel films are quite different in structure and properties to polymers. It is reasonable to expect that the solubility may also be different. Table 6.8 shows solubility estimates for the two sol-gel films discussed in Section 6.2, where S was calculated using Equation 6.2. For comparison, solubility values are also given for a silicon rubber and polystyrene film, this data was calculated using literature values for $K_{SV}$, $\tau_0$ and D for the two films.

| Film | $K_{SV}$ $(Torr^{-1})$ | $\tau_0(\mu s)$ | D$(cm^2 s^{-1})$ | S$(Pa^{-1})$ |
|---|---|---|---|---|
| TEOS R=4 | .004605 | 5.1 | $3.5 \times 10^{-9}$ | $4 \times 10^{-4}$ |
| MTEOS R=2 | .004267 | 4.9 | $7.8 \times 10^{-8}$ | $1.7 \times 10^{-5}$ |
| Silicone RTV 118 | .033 | 5 | $12 \times 10^{-6}$ | $1.3 \times 10^{-6}$ [6, 8] |
| Polystyrene | .00092 | 5.3 | $1.87 \times 10^{-7}$ | $2 \times 10^{-6}$ [8, 9, 10] |

**Table 6.8:** Comparison of solubility results for TEOS, MTEOS and polymer films

It is clear from Table 6.8 that there is an order of magnitude increase in solubility between the polymer films and the MTEOS films while TEOS has an even larger value. This large value of S for the TEOS film is implied as a result of the relatively small diffusion coefficient given that $K_{SV}$ for all sol-gel films are of the same order. It is suggested that the order of magnitude increase in solubility for sol-gel films compared to polymer films arises from the relatively rigid nature of the sol-gel structure characterised by a large number of micropores resulting in a large free volume. The intermediate value for solubility for MTEOS is consistent with the hybrid nature of the ormosil film where the structure is less rigid and more polymer-like but with more free volume than a typical polymer film. The difficulties relating to measuring the absolute porosity of MTEOS have been highlighted previously. However, from the literature, it is likely that the porosity is less than that of TEOS. This is consistent with lower oxygen solubility.

Thus it is the effect of the solubility, S, that leads TEOS and MTEOS films to have approximately the same value of $K_{SV}$, while significant differences are seen in the diffusion coefficients.

As highlighted in Chapter 1, much has been published on sol-gel derived films for oxygen sensor applications. As well as the inherent advantages of the sol-gel films over polymer films, such as superior optical quality and mechanical properties as well as the ability to tailor the properties and increased coating flexibility, the oxygen

sensitivity is in the same range as many widely used polymers. In the context of tailoring sensor films for optimum oxygen sensitivity, it is interesting to note that, while many polymers film have larger diffusion coefficients, as seen in Table 6.8, Stern-Volmer coefficients for most polymer films are comparable with those of sol-gel films. Apart from RTV rubber which has a very high $K_{SV}$ ($2.5 \times 10^{-4}$ $Pa^{-1}$ with Ru(dpp) complex) many polymers, which have been widely used in oxygen sensing using the same ruthenium complex, have $K_{SV}$ values in the range $10^{-5}$ $Pa^{-1}$. It is clear from this work that the increased oxygen solubility for sol-gel films enhances the overall oxygen sensitivity and compensates somewhat for the lower sol-gel diffusion coefficients.

## 6.4 Response times and diffusion coefficients when going from $N_2$ to $O_2$ environment

The data reported so far was obtained when the sol-gel thin films were exposed to alternative environments of vacuum and $O_2$. It is more important to evaluate response times for changing $O_2$ concentrations at ambient pressure. Tables 6.9 and 6.10 show the response times for a range of TEOS and MTEOS films exposed to the two different environments investigated ($O_2$/vacuum and $N_2/O_2$ at ambient pressure).

In order to make the ambient pressure measurements, the same experimental procedure as described in Section 4.8 was used, the only difference being the fact that the vacuum was replaced with a $N_2$ supply.

| Sample | Aging Time (hours) | $t_{90}$ Vacuum (ms) | $t_{90}$ $N_2$ (ms) |
|---|---|---|---|
| TEOS R=2 | 4 | 106 | 906 |
| | 6 | 77.8 | 424 |
| | 16 | 40.2 | 149 |
| TEOS R=4 | 6 | 538.8 | 853 |
| | 16 | 462 | 642 |

**Table 6.9:** Comparison between response times between a $O_2$/vacuum and a $N_2/O_2$ environment, for a range of TEOS films

From Tables 6.9 and 6.10 it can be seen that longer response times were measured for films when going from $N_2$ to $O_2$. It can be assumed that under vacuum the pore

| Sample | $t_{90}$ Vacuum (ms) | $t_{90}$ $N_2$ (ms) |
|---|---|---|
| MTEOS R=2 | 10.2 | 34.5 |
| MTEOS R=4 | 19.2 | 71.0 |

**Table 6.10:** Comparison between response times between a $O_2$/vacuum and a $N_2/O_2$ environment for a range of MTEOS films

structure of the sol-gel film is devoid of gas molecules. Hence, when $O_2$ interacts with the film, the molecules find it easier to travel through the pore structure and interact with the Ru(dpp) dye resulting in rapid quenching of fluorescence. In the case of the film being exposed to alternative environments of $N_2$ and $O_2$, the pores are full with a given gas that has to be expelled from the matrix structure in order for the other gas to interact with the Ru(dpp) dye. This results in the gases diffusing through the matrix at a slower rate leading to longer response times.

Using the model described in Section 3.5, diffusion coefficients were calculated for a number of films when the atmosphere was alternating between $N_2$ and $O_2$.

From Tables 6.11 and 6.12, it can be seen that the diffusion coefficients of sensor films are affected when measurements are made at ambient pressure. The diffusion coefficients are generally smaller than previously calculated for the same reason as proposed with respect to the response times.

| Sample | Aging Time (hours) | D($cm^2s^{-1}$) Vacuum | D($cm^2s^{-1}$) $N_2$ |
|---|---|---|---|
| TEOS R=2 | 4 | $5.0 \times 10^{-9}$ | $5.0 \times 10^{-10}$ |
| | 6 | $1.5 \times 10^{-8}$ | $1.2 \times 10^{-9}$ |
| | 16 | $3.2 \times 10^{-8}$ | $2.2 \times 10^{-9}$ |
| TEOS R=4 | 6 | $3.5 \times 10^{-9}$ | $2.5 \times 10^{-10}$ |
| | 16 | $8.8 \times 10^{-9}$ | $6.2 \times 10^{-10}$ |

**Table 6.11:** Comparison between diffusion coefficient calculated for vacuum/$O_2$ and $N_2/O_2$ environments for TEOS R=2 and 4

| Sample | D($cm^2s^{-1}$) Vacuum | D($cm^2s^{-1}$) $N_2$ |
|---|---|---|
| MTEOS R=2 | $7.8 \times 10^{-8}$ | $1.2 \times 10^{-8}$ |
| MTEOS R=4 | $5.9 \times 10^{-8}$ | $8.7 \times 10^{-9}$ |

**Table 6.12:** Comparison between diffusion coefficient calculated for vacuum/$O_2$ and $N_2/O_2$ environments for MTEOS R=2 and 4

## 6.5 Conclusion

Response times were measured for a range of sol-gel films. However the intrinsic response time, 5ms, of the solenoid valve has to be taken into account when analysing response times. Using these response time values the diffusion coefficients were measured. The porosity, response time and diffusion coefficients were correlated. For all samples it was seen that an increase in porosity led to a higher diffusion coefficient and shorter response times. However MTEOS films proved to have the highest diffusion coefficients and shorter response times even though the films are dense when compared to TEOS-based films.

This proved to be due to the hydrophobic/hydrophilic nature of the surface of the film. TEOS has a hydrophilic surface where water molecules bond to the pore surface, reducing the effective porosity of the sample. As a result the $O_2$ molecules diffuses through the sample at a slower rate leading to slower response times. MTEOS, on the other hand is hydrophobic, meaning little or no water molecules can bond to the surface leaving an easy accessible path for the $O_2$ to diffuse through the film and interact with the oxygen sensitive ruthenium complex.

Stern-Volmer coefficients, $K_{SV}$, measured from the straight line Stern-Volmer graph, were correlated with diffusion coefficients. Again a difference in the behavior of MTEOS films was noticed. Comparing TEOS and MTEOS samples with approximately the same value of $K_{SV}$, it was noted that there was a factor of 20 between the diffusion coefficients, MTEOS having the higher value. This discrepancy was interpreted in terms of oxygen solubility of the films. While both film types exhibit similar oxygen permeability behavior and have similar optical decay times, the larger MTEOS diffusion coefficient is indicative of a lower value for oxygen solubility. This behavior is consistent with he microstructural differences between the two film types.

To examine the sensors behavior in a more realistic situation the vacuum was replaced by $N_2$ gas. The response times proved to be longer with smaller diffusion coefficients.

# Bibliography


[1] P. Innocenzi, M.O. Abdirashid, and M. Guglielmi. Structure and properies of sol-gel coatings from methyltriethoxysilane and tetraethoxysilane. *Journal of Sol-Gel Science and Technology*, 3:47–55, 1994.

[2] H. Schmidt, H. Scholse, and A. Kaiser. *Journal of Non-Crystalline Solids*, 63:1, 1984.

[3] N.D. Koone and T.W. Zerda. Diffusion and optical proties of Nd-doped sol-gel silica glasses. *Journal of Non-Crystalline Solids*, 183:243–251, 1995.

[4] W. Xu, R. Schmidt, M. Whaley, J.N. Demas, B.A. DeGreaff, E.K. Karikari, and B.L. farmer. Oxygen sensors based on luminescence quenching: Interactions of pyrene with the polymer supports. *Analytical Chemistry*, 67:1377–1380, 1995.

[5] K. Mongey, JG Vos, B.D. Maccraith, and C. McDonagh. The photophysical properties of ruthernium polypyridyl complexes within a sol-gel matrix. *Journal of Sol-Gel Science and Technology*, 8:979–983, 1997.

[6] A. Mills. Controlling the sensitivity of optical oxygen sensors. *Sensors and Actuators B*, 51:60–68, 1998.

[7] C. McDonagh, P. Bowe, K. Mongey, and B.D. MacCraith. Characterisaction of porosity and sensor response times of sol-gel derived thin films for oxygen sensor applications. *Journal of Non-Crystalline Solids*, 306:138–148, 2002.

[8] E.R. Carraway, J.N. Demas, B.A. Degraff, and J.R. Bacon. Photophysics and photochemistry of oxygen sensors based on luminescent transition-metal complexes. *Analytical Chemistry*, 63:337–342, 1991.

[9] M.A. Winnik, Y. Rharbi, and A. Yekta. A method for measuring oxygen diffusion and oxygen permeation films based on fluorescence quenching. *Analytical Chemistry*, 71:5045–5053, 1999.

[10] I. Klimant, K. Ruckruh, G. Liebsch, A. Stangelmayer, and O.S. Wolfbeis. *Mikrochimica Acta*, 131:35, 1999.

# Chapter 7

# Investigation of oxygen sensitivity of other matrix types

## 7.1 Introduction

This chapter deals with the oxygen sensitive metal complex, Ru(dpp), immobilised in different matrices, namely soluble ormosils, phenyl-based matrices and a combination of TEOS and MTEOS mixed together in different ratios. In each case the films were characterised, by measuring the Stern-Volmer and diffusion coefficients as well as the sensor response time.

Hydrophobic sol-gel based organically modified precursors avoid the penetration of water into the matrix. Such materials are suitable for embedding indicators, for sensing dissolved gaseous species such as oxygen.

The introduction of the methyl groups (MTEOS) results in a lower degree of crosslinking (lower porosity) and an increase in the hydrophobicity of the surface of the material. It was decided to investigate the characteristics of oxygen-sensitive films, resulting from the hydrolysis and condensation of a mixture of MTEOS and TEOS combined together in different ratios.

Recently, modified silica materials have begun to receive attention for integrated optics applications [1, 2, 3]. Organically modified silica has the potential advantage of being cost efficient and readily adjustable composition. Moreover ormosil films of the required thickness can be deposited in a single step. They can also be made photosensitive for direct UV writing of waveguides and the processing temperatures <100°C may enable direct integration with semiconductor sources and detectors.

If, at any stage in the future, an oxygen sensitive sol-gel film were to be incorporated into a silica-based integrated optical circuit, to ensure compatibility, control of the refractive index will be required. One such method to control refractive index is to modify the TEOS-based silica with phenyl groups. By changing the quantity of the phenyl precursors in the sol composition, the refractive index can be easily controlled and modified. Methyl groups can also be added to the sol to produce films with the desired refractive index and good crack resistance. During the investigation of these films, the dependence of refractive index and thickness on phenyl content was investigated. The $O_2$-sensitive metal complex Ru(dpp) was incorporated into the films and their performance as oxygen sensitive films was also investigated.

A new type of soluble ormosil as a matrix for oxygen sensitive films was also investigated. The ormosil was synthesised according to a formulation that was developed at the University of Regensburg in Germany by Klimant et al. [4]. The new ormosil combines features of polymers such as solubility in organic solvents and those of sol-gel glasses such as mechanical stability and a porous structure, that allows them to be doped with indicator dyes, such as Ru(dpp). In this study the response times and the Stern-Volmer and diffusion coefficients of these films is also reported.

## 7.2 Investigation of films fabricated using TEOS and MTEOS mixed together in different molar ratios

Films were prepared as described in Section 4.4.2, in the ratio of MTEOS:TEOS of 2:1, 3:1 and 4:1. Table 7.1 shows the calculated diffusion coefficients and response times associated with these films.

| MTEOS:TEOS Ratio | $t_{90}$ (ms) | D ($cm^2 s^{-1}$) |
|---|---|---|
| 2:1 | 39.9 | $7.29 \times 10^{-8}$ |
| 3:1 | 26.6 | $9.0 \times 10^{-8}$ |
| 4:1 | 24.5 | $2.38 \times 10^{-7}$ |

**Table 7.1:** Diffusion coefficients and response times of films fabricated using different molar ratios of MTEOS and TEOS

From the results it can be seen that response times become shorter as the

MTEOS:TEOS ratio increases even though the films become more dense and the porosity decreases [5]. This is probably due to the hydrophobic nature of MTEOS. The film surface increases in hydrophobicity as the MTEOS content increases, ensuring that less and less water is adsorbed onto the pore surface. The $O_2$ molecules access the quenching sites more easily as the film surface increases in hydrophobicity. The ease of passage of $O_2$ molecules with increasing methyl content is also reflected in the diffusion coefficients, where the calculated diffusion coefficients were found to increase with increasing MTEOS:TEOS ratio.

## 7.3 Investigation of films fabricated using phenyl-substituted films

The refractive index and thickness of a range of doped phenyl-substituted films was investigated, namely MTEOS/PhTEOS/TEOS and MTMOS/PhTEOS/
TEOS in the ratios of x/(80-x)/20 and x/(60-x)/40. The refractive index and thickness was measured using the Metricon prism coupler as previously described in Section 4.9. Figures 7.1 and 7.2 show the dependence of refractive index on phenyl content.

From Figure 7.1 and 7.2, it can be seen that the refractive index increases sub-linearly with phenyl content to a limit of approximately 1.55. This is in agreement with data reported by other authors [1, 6, 7].

In agreement with Atkins and Vorotilov [1, 6] we assigned the refractive index increase effect to the high polarisability ($\pi$-bonding electrons) and the high refractive index of phenyl radicals. The sub-linear nature of the refractive index is linked to a decrease in density (i.e. increase in porosity) arising from steric hindrance of silanol condensation by the phenyl groups. From the presented data it can be seen that for a given total content of tri-functional ethoxysilanes in the starting solution, a specific refractive index in the range 1.47-1.55 can be achieved by simply adjusting the relative amounts of precursors.

Figures 7.3 and 7.4 shows the thicknesses measured for MTEOS/PhTEOS/TEOS and MTMOS/PhTEOS/TEOS in the molar ratios x/(80-x)/20 and x/(60-x)/40.

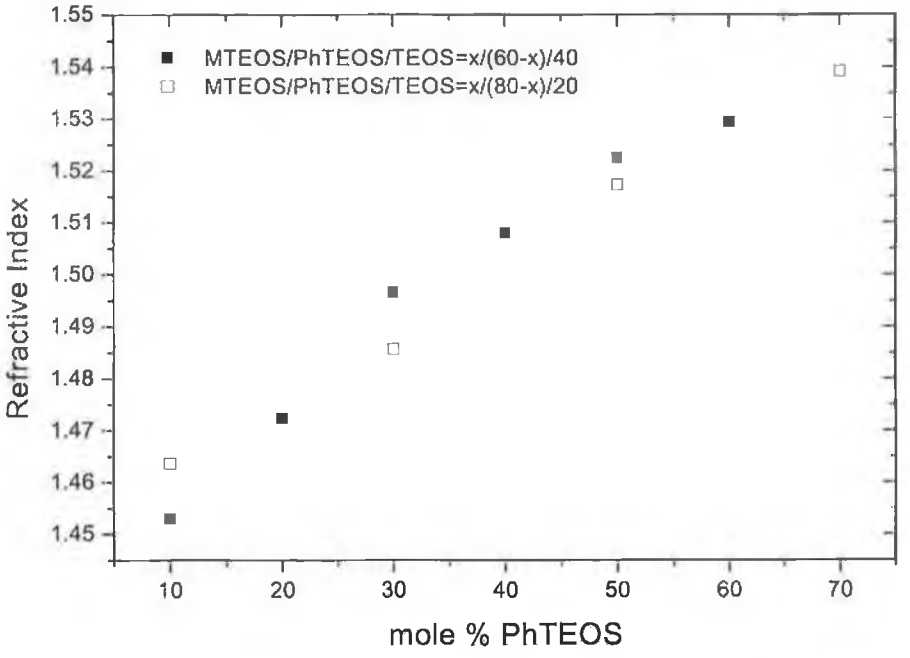


**Figure 7.1:** Shows the refractive index of MTEOS/PhTEOS/TEOS= (80-x)/x/20 and (60-x)/x/40, as a function of mole % PhTEOS

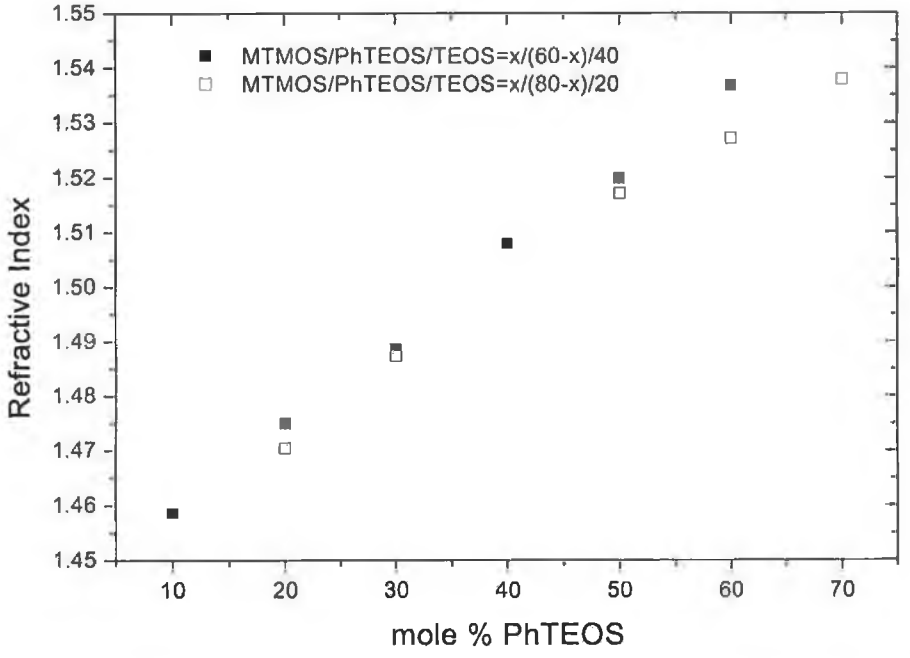


**Figure 7.2:** Shows the refractive index of MTMOS/PhTEOS/TEOS= x/(80-x)/20 and x/(60-x)/40, as a function of mole % PhTEOS

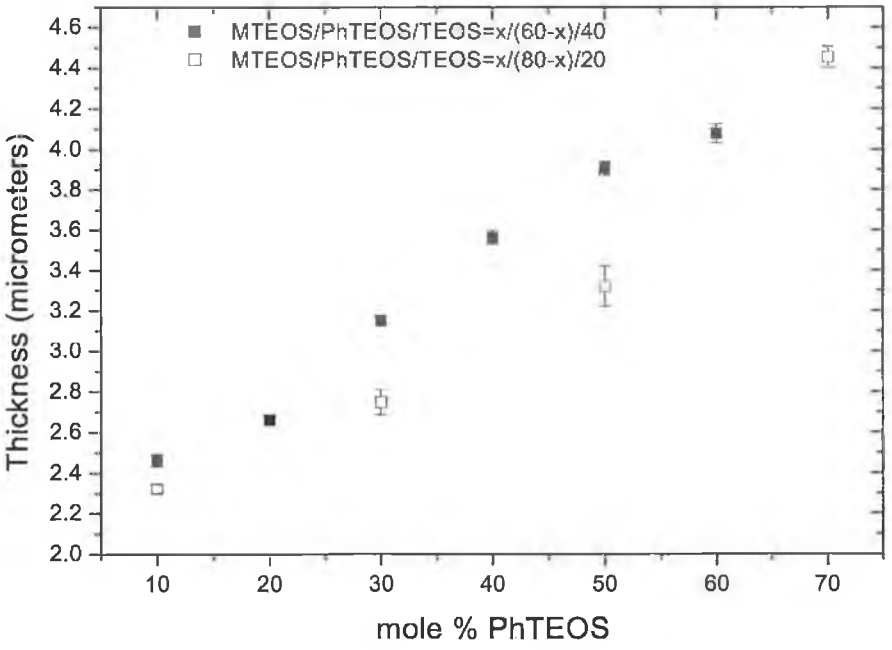


**Figure 7.3:** Shows the thickness of MTEOS/PhTEOS/TEOS=x/(80-x)/20 and x/(60-x)/40

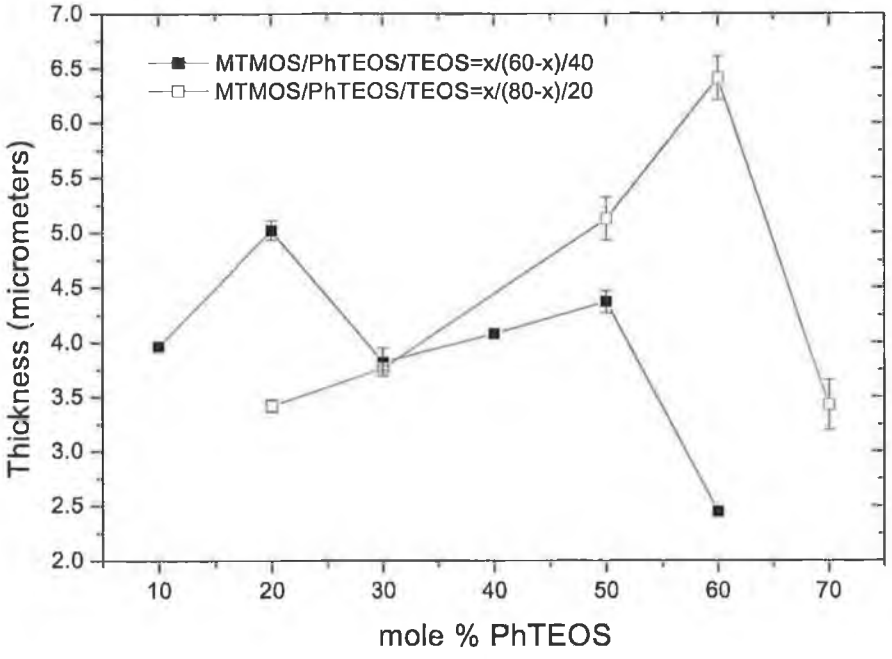


**Figure 7.4:** Shows the thickness of MTMOS/PhTEOS/TEOS= x/(80-x)/20 and x/(60-x)/40

As seen from Figure 7.3, relatively thick films are achievable at a dip speed of 3mm/s, with film thickness increasing with increasing phenyl content. Also from Figure 7.3 a maximum thickness of approximately 4$\mu$m is achievable when the precursors MTEOS/PhTEOS/TEOS are combined together.

It is difficult to extract a trend from Figure 7.4. Films fabricated from MTMOS/PHTEOS/TEOS=x/(80-x)/20 show an increase in thickness from approximately 3.25 to 6.4$\mu$m with increasing phenyl content. However, above a molar phenyl content of 60%, the thickness is seen to decrease dramatically to approximately 3$\mu$m.

The thickness values of films fabricated from MTMOS/PhTEOS/TEOS=x/(60-x)/40 also behave in a strange manner. The thickness increases as expected when the PhTEOS molar content increases from 10 to 20%. The thickness then decreases when a PhTEOS molar content of 30% is used. The thickness then increases again when a PhTEOS molar content greater than 30% is used. But above 50% PhTEOS molar content the thickness decreases again to approximately 2.25$\mu$m.

The reason for the decrease in thickness above a certain molar % of PhTEOS is unknown, but Vorotilov et al. [6] showed that the amount of film shrinkage during the drying process depended on phenyl content. Furthermore a decrease in thickness was only seen when MTMOS was used.

Therefore the presence of MTMOS in conjunction with PhTEOS must dramatically effect the shrinkage process of the film during drying, resulting in a decrease in thickness for films above a certain % molar content of PhTEOS.

### 7.3.1 Film characterisation of phenyl-substituted oxygen sensitive films

As already described in Section 4.3, Ru(dpp) was incorporated into the phenyl-substituted ormosil films. Tables 7.2 and 7.3 show the response time, Stern-Volmer and diffusion coefficients and the thickness of films prepared using the precursors MTEOS, MTMOS, PhTEOS and TEOS.

A large amount of information is contained in Tables 7.2 and 7.3 and one can deduce a lot from this. It can be seen that as phenyl content increases it leads to thicker films resulting in films with longer response times as expected.

| mole % PhTEOS | $t_{90}$ (ms) | $K_{SV}$ $(Torr^{-1})$ | D $(cm^2s^{-1})$ | Thickness ($\mu$m) |
|---|---|---|---|---|
| 10 | 374 | .00177 | $7.65 \times 10^{-8}$ | 2.32 |
| 30 | 505 | .00247 | $8.30 \times 10^{-8}$ | 2.75 |
| 50 | 524 | .00378 | $1.20 \times 10^{-7}$ | 3.32 |
| 60 | 575 | .00401 | $2.47 \times 10^{-7}$ | 4.45 |
| 70 | 579 | .00408 | $2.47 \times 10^{-7}$ | 4.45 |

**Table 7.2:** Response time, Stern-Volmer coefficient, diffusion coefficient and thickness of films fabricated using the precursors MTEOS, PhTEOS and TEOS in the ratio of x/(80-x)/20

| mole % PhTEOS | $t_{90}$ (ms) | $K_{SV}$ $(Torr^{-1})$ | D $(cm^2s^{-1})$ | Thickness ($\mu$m) |
|---|---|---|---|---|
| 10 | 510 | .00265 | $1.20 \times 10^{-7}$ | 3.58 |
| 30 | 578 | .00336 | $1.69 \times 10^{-7}$ | 3.77 |
| 50 | 764 | .00392 | $1.84 \times 10^{-7}$ | 5.13 |
| 60 | 828 | .00481 | $4.58 \times 10^{-7}$ | 6.41 |

**Table 7.3:** Response time, Stern-Volmer coefficient, diffusion coefficient and thickness of films fabricated using the precursors MTMOS, PhTEOS and TEOS in the ratio of x/(80-x)/20

It can be seen that an increase in the Stern-Volmer and diffusion coefficients coincides with an increase in the phenyl content of the films. This is expected, as Atkins et al. [1] have shown previously that porosity increases with phenyl content. Comparison of films with similar phenyl contents, shows that films fabricated using MTMOS/PhTEOS/TEOS mixtures exhibit higher values of Stern-Volmer and diffusion coefficients, resulting in films with a higher value of oxygen sensitivity, although with longer response times.

Films were also fabricated using a mixture of two precursors. These were mixtures of either PhTEOS/TEOS and PhTEOS/MTEOS. The films were fabricated as described in Section 4.3. From Tables 7.4 and 7.5, it can be seen that the Stern-Volmer and diffusion coefficients increase with phenyl content.

When comparing films in Tables 7.4 and 7.5 with similar phenyl-content, it can be seen that films fabricated from a PhTEOS/MTEOS combination have better oxygen sensing attributes with higher Stern-Volmer and diffusion coefficients and shorter response times than those fabricated from PhTEOS/TEOs combination. This represents an important strategy in the tailoring if films for different sensing applications.

| PhTEOS/TEOS | | | | |
|---|---|---|---|---|
| mole % PhTEOS | $t_{90}$ (s) | $K_{SV}(Torr^{-1})$ | D$(cm^2s^{-1})$ | Thickness($\mu$m) |
| 20 | .76 | .00153 | $9.4 \times 10^{-8}$ | 3.03 |
| 40 | .802 | .00308 | $1.04 \times 10^{-7}$ | 4.46 |
| 60 | .830 | .00359 | $1.98 \times 10^{-7}$ | 5.63 |
| 80 | 1.51 | .00412 | $2.63 \times 10^{-7}$ | 7.58 |

**Table 7.4:** Response time, Stern-Volmer coefficient, diffusion coefficient and thickness of oxygen sensitive films fabricated using the precursors PhTEOS and TEOS in different ratios

| PhTEOS/MTEOS | | | | |
|---|---|---|---|---|
| mole % PhTEOS | $t_{90}$ (ms) | $K_{SV}(Torr^{-1})$ | D$(cm^2s^{-1})$ | Thickness($\mu$m) |
| 20 | 187 | .00256 | $1.39 \times 10^{-7}$ | 1.93 |
| 40 | 485 | .00343 | $3.10 \times 10^{-7}$ | 4.70 |
| 60 | 791 | .00391 | $3.39 \times 10^{-7}$ | 7.72 |
| 80 | 841 | .00446 | $3.92 \times 10^{-7}$ | 7.97 |

**Table 7.5:** Response times, Stern-Volmer coefficient, diffusion coefficient and thickness of oxygen sensitive films fabricated using the precursors PhTEOS and MTEOS in different ratios

## 7.4 Soluble ormosils

Soluble ormosil oxygen-sensitive films were prepared as described in Section 4.4.1. Table 7.6 shows the resulting film characteristics.

| Sample | $t_{90}$ (ms) | $K_{SV}$ $(Torr^{-1})$ | D$(cm^2s^{-1})$ | Thickness ($\mu$m) |
|---|---|---|---|---|
| Soluble Ormosil | 189 | .00508 | $4.76 \times 10^{-8}$ | 1.1 |

**Table 7.6:** Characteristics of an oxygen sensitive soluble ormosil based on average values of 3 films.

From Table 7.6, the soluble ormosils show favorable properties such as high Stern-Volmer and diffusion coefficients, that are comparable to those of MTEOS and TEOS oxygen sensitive films.

However, the soluble ormosils have a number of advantages over regular sol-gel derived glass. The reproducible fabrication of stable sensor matrices with sol-gel as a matrix is not as simple as often described. The advantage of a matrix that may be tailored by slight variation of parameters during polymerisation turns out to be a disadvantage with respect to obtaining materials with identical sensing properties. Furthermore, sensors based on sol-gel entrapped indicators are frequently not stable over time. However the fabricated soluble ormosils investigated in this

section offer reproducible values for the Stern-Volmer and diffusion coefficients as well as short response times. The films can also be fabricated with an excellent batch to batch reproducibility [4]. As a result the soluble ormosil films posses good oxygen sensitivity, short response times and good film reproducibility.

## 7.5 Conclusion

Response times and Stern-Volmer coefficients were measured for a range of sol-gel films. Using the response times, the diffusion coefficients were calculated.

The investigation of MTEOS:TEOS films combined together in different molar ratios show that as the MTEOS:TEOS ratio increases, the response time reduces. Also the diffusion coefficient increases with an increase in the MTEOS:TEOS ratio, even though increasing the presence of methyl-groups in a sol-gel based film result in a decrease in porosity. This is probably due to the oxygen molecules accessing the quenching site more easily as the film surface increases in hydrophobicity with increasingly methyl content.

Films were also fabricated using a combination of the precursors MTEOS, MTMOS, PhTEOS and TEOS. The refractive index increases with an increase in phenyl content, to a limit of approximately 1.55. The sub-linear nature of the increase of the refractive index is attributed to an increase in porosity. Thickness measurements were also made on the films and crackfree films of up to approximately 6.5$\mu$m were achievable. As with refractive index measurements, the thickness was noted to increase with phenyl content.

It is clear from the results that phenyl-substituted silica offers some advantages for oxygen sensing, with the Stern-Volmer and diffusion coefficients comparable to that of other sol-gel based oxygen sensitive films. In addition the control of refractive index and thickness allows for the future integration with semiconductor sources and detectors.

The fabrication of soluble ormosils provided films with a short response time and a diffusion coefficient comparable to that of other sol-gel materials. The Stern-Volmer coefficient for the films is large, .00508 Torr$^{-1}$, indicating that these ormosil films are attractive for oxygen sensing.

The main advantage of soluble ormosils over other sol-gel-derived thin films is that sensors with easily reproducible properties (Stern-Volmer and diffusion coef-

ficients) can easily be reproduced from a single batch. Moreover the hydrophobic nature of the soluble ormosil avoids the penetration of water into the matrix, thus making it suitable for aqueous sensing applications.

# Bibliography

[1] G.R. Atkins, R.M. Krolikowska, and A. Samoc. Optical propteries of an ormosil system comprising methyl- and phenyl-substituted silica. *Journal of Non-Crystalline Solids*, 265:210–220, 2000.

[2] D.L. Ou and A.B. Seddon. Structural investigation of ormosils with potential as host photonic materials. *Journal of Sol-Gel Science and Technology*, 8:139, 1997.

[3] D.L. Ou and A.B. Seddon. Near- and mid-infrared spectroscopy of sol-gel derived ormosils: vinyl and phenyl silicates. *Journal of Non-Crystalline Solid Solids*, 210:187, 1997.

[4] I. Klimant, F. Ruckruh, G. Liebsch, A. Stangelmayer, and O.S. Wolfbeis. Fast response oxygen micro-opodes based on novel soluble ormosil glasses. *Mikrochimica Acta*, 131:35–36, 1999.

[5] P. Innocenzi, M.O. Abdirashid, and M. Guglielmi. Structure and properies of sol-gel coatings from methyltriethoxysilane and tetraethoxysilane. *Journal of Sol-Gel Science and Technology*, 3:47–55, 1994.

[6] K.A. Vorotilov, V.A Vasiliev, M.V. Sobolevsky, and A.S. Sigov. Thin ormosil films with different organics. *Journal of Sol-Gel Science and Technology*, 13:467–472, 1998.

[7] K.A. Vorotilov, V.I. Petrovsky, V.A. Vasiljev, and M.V. Sobolevsky. Ormosil films: Properties and microelectric applications. *Journal of Sol-Gel Science and Technology*, 8:581–584, 1997.

# Chapter 8

# Conclusions

The work presented in this thesis describes the characterisation of sol-gel derived thin films for optical oxygen sensing. The sensing process is based on the quenching of fluorescence from ruthenium metal complexes. In this work, Ru(II) tris(4-7-diphenyl-1, 10-phenanthroline) was chosen as the sensing species due to its long lifetime ($\approx 5\mu s$) and its strong absorption in the blue-region of the spectrum.

The sol-gel process and the parameters that control the rates of the chemical reactions involved, were described. Using the sol-gel method as an immobilisation technique is an inherently easy process to carry out. It offers the possibility of controlling the physical and chemical nature of the final structure by controlling various reaction parameters.

Experimental systems to measure both the response time and porosity as well as a computer model to calculate the diffusion coefficient were developed and perfected.

From the wide range of fabricated sol-gel derived films the porosity was consistent with the microstructural behavior predicted as a function of fabrication parameters such as pH, aging time and R-value. As expected, the porosity of TEOS films proved greater than MTEOS films. The porosity results indicate the ease with which the sol-gel matrix can be tailored and modified.

For a given film type, the oxygen diffusion coefficient correlated directly with the Stern-Volmer constant, which in turn was related to porosity and response time. However, MTEOS films proved to have a higher diffusion coefficients and shorter response times even though they are more dense when compared to TEOS. This is due to the hydrophobic/hydrophilic nature of the film surface, where a hydrophilic surface leads to a layer of water forming on the TEOS film surface. This results

in oxygen molecules having to partition into and out of a layer of water as they move through the sol-gel film leading to longer response times and smaller diffusion coefficients when compared to hydrophobic MTEOS.

The diffusion coefficient of MTEOS films exhibited more than a 20-fold increase compared with that of TEOS films for films of similar Stern-Volmer constant. This discrepancy was interpreted in terms of oxygen solubility of the films. While both films exhibit similar oxygen permeability behavior and have similar optical decay times, the larger MTEOS diffusion coefficient is indicative of a lower value for oxygen solubility. This behavior is consistent with the microstructural differences between the two film types. This enhanced solubility of sol-gel films compared to many polymers reinforces the important role played by sol-gel films optical oxygen sensor applications.

Sol-gel derived optical oxygen sensors were evaluated to measure response times for changing $O_2$ concentrations at ambient pressure. The response times proved to be longer with smaller diffusion coefficients.

In the case of this work, a more fundamental understanding of the detailed effects of solubility, porosity, response time, diffusion coefficients and Stern-Volmer coefficients has on sol-gel derived thin film optical oxygen sensing has been gained.

Future work could include a more detailed study of the solubility mechanisms for oxygen in sol-gel films. This would include a further study of solubility over a wider range of sol-gel derived thin films.

# Appendix A

# List of Publications and Conference Presentations

**Publications:**

i) Colette McDonagh, Philip Bowe, Karen Mongey, Brian MacCraith, 'Characterisation of porosity and sensor response times of sol-gel derived thin films for oxygen sensor applications', *Journal of Non-Crystalline Solids*, 306, 2002, pp. 138-148

**Poster Presentations**

i) Characterisation of microporous films for optical oxygen sensing', Europt(r)ode V, Opt(r)rode, 16-19 April 2000, Lyon-Villeurbanne, France.

ii) Characterisation of sol-gel derived porous films for optical oxygen sensing', 4th UK-Ireland Sol-Gel Meeting, 11-12 September 2000, Nottingham Trent University England.

**Oral Presentation**

i) Sol-Gel-Derived Films for Optical Gas Sensing: Porosity and Response Time Issues', XI International Workshop on Glasses, Ceramics Hybrids and Nanocomposities from Gels, 16-21 September 2001, Abano Terme, Padova, Italy.

# Appendix B

# Program code used to calculate the diffusion coefficient

```
#include <iostream.h>
#include <math.h>
#include <values.h>
#include <fstream.h>

int main ()

{

//Declaring the variables

int n,count,count1; char filename1[12], filename2[12],
filename3[12], filename4[12], newfile;

float q,x,t,theta,D,l,c,I,avg_in,avg_out,tau; long double
sum,sum2,sum3,w,w1,s,s1,totalin=0,totalout=0;

fstream s_in,s_out,a_in,a_out;
```

```
//Declaring the input values and filenames

cout <<"tau:";
cin >> tau;

cout << "Thickness:";
cin >> l;

cout <<"Enter concentration value:";
cin >> c;

cout <<"Filename for in data:";
cin >> filename1;

cout<<"Filename for out data:";
cin >> filename2;

cout << "Filename for average in values:";
cin >> filename3;

cout <<"Filename for average out values:";
cin >> filename4;

cout <<"Do you want to use these as new files(y/n):";

cin>>newfile;

s_in.open(filename1, ios:: beg | ios :: out);
s_out.open(filename2,ios:: beg | ios :: out);

if (newfile =='y')

    {
    a_in.open(filename3, ios:: beg | ios :: out);
```

```
s_in << x/l <<' '<< s <<' '<<endl; totalin+=s;
//accumulate total for average value

s_out << x/l <<' '<< s1 <<' '<<endl; totalout+=s1;
    }


//calculates average values

avg_in=(totalin/499); avg_out=(totalout/499);

a_in <<tau<<' ' << avg_in<<endl;

cout<< "average for in tau=" <<tau<<" :" <<avg_in<<endl;

a_out <<tau<<' ' << avg_out<<endl;

cout<< "average for out tau=" <<tau<<" :" <<avg_out<<endl;

s_in.close(); s_out.close(); a_in.close(); a_out.close();

return 0;

}
```

```
    a_out.open(filename4, ios:: beg | ios :: out);
    }

else
    {
    a_in.open(filename3, ios:: app | ios :: out);
    a_out.open(filename4, ios:: app | ios :: out);
    }

//calculates the sum


for (x=0; x<=l; x++)


    {
    cout << '>';
    sum=0;
    for(n=0;n<1000;n++)

{
        theta=2*n+1;

        sum+=pow(-1,n)* pow(theta,-1)*
        exp(-1*theta*theta*M_PI*M_PI*tau/4)*
        cos(theta*M_PI*x/(l*2));

        }

//calculates the fractional change in optical signal

s=(4/M_PI)* sum/ (1+c* (1-(4/M_PI)* sum)); s1=(1-(4/M_PI)*
sum)/(1+c*(4/M_PI)* sum);
```

# Appendix C

# Block diagram of Labview program used to acquire signal from photodiode

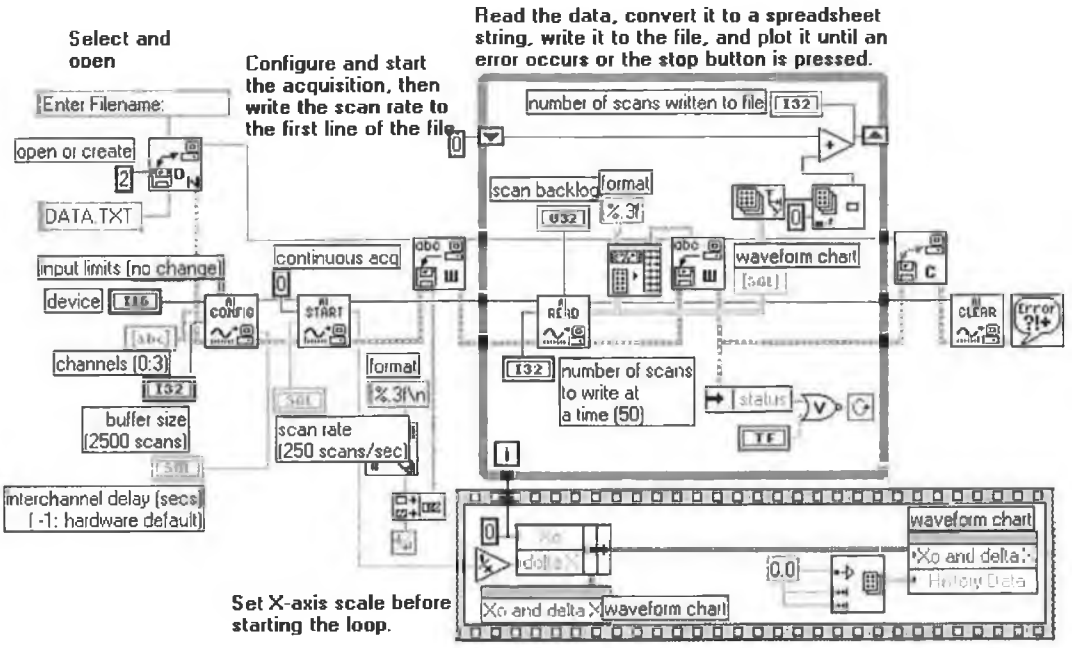

# Appendix D

# Block Diagram of Labview program used to control the solenoid valve